Clim Dyn (2017) 49:1705–1727
DOI 10.1007/s00382-016-3393-z

Time-varying spectral characteristics of ENSO over the Last Millennium

Pandora Hope[1] · **Benjamin J. Henley**[2] · **Joelle Gergis**[2] · **Josephine Brown**[1] · **Hua Ye**[1]

Received: 20 September 2015 / Accepted: 6 October 2016 / Published online: 26 October 2016

Abstract The characteristics of El Nino–Southern Oscillation (ENSO) spectra over the Last Millennium are examined to characterise variability over past centuries. Seven published palaeo-ENSO reconstructions and Nino3.4 from six Coupled Model Intercomparison Project-Phase 5 and Paleoclimate Modelling Intercomparison Project-Phase 3 (CMIP5–PMIP3) Last Millennium simulations were analysed. The corresponding Historical and pre-industrial Control CMIP5–PMIP3 simulations were also considered. The post-1850 spectrum of each modelled or reconstructed ENSO series captures aspects of the observed spectrum to varying degrees. We note that no single model or ENSO reconstruction completely reproduces the instrumental spectral characteristics. The spectral power across the 2–3 years (near biennial), 3–8 years (classical ENSO) and 8–25 years (decadal) periodicity bands was calculated in a sliding 50 year window, revealing temporal variability in the spectra. There was strong temporal variability in the spectral power of each periodicity band in observed Nino3.4 and SOI and for all reconstructions and simulations of ENSO. Significant peaks in spectral power such as observed in recent decades also occur in some of the reconstructed palaeo-ENSO (around 1600, the early 1700s and 1900) and modelled series (around the major volcanic eruptions of 1258 and 1452). While the recent increase in spectral power might be in response to enhanced greenhouse gas levels, the increase lies within the range of variability across the suite of ENSO reconstructions and simulations examined here. This study demonstrates that the analysis of a suite of ENSO reconstructions and model simulations can build a broader understanding of the time-varying nature of ENSO spectra, and how the nature of the past spectra of ENSO is to some extent dependant on the climate model or palaeo-ENSO reconstruction chosen.

Keywords El Niño–Southern Oscillation · ENSO · SOI · Nino3.4 · Last Millennium · Climate model simulations · Spectra · CMIP5 · PMIP · Decadal variability

1 Introduction

The El Niño–Southern Oscillation (ENSO) is the major coupled ocean–atmospheric phenomenon driving global climate variability on interannual timescales (Bjerknes 1966, 1969; Allan et al. 1996). ENSO variability can be measured with a range of indices, such as the Southern Oscillation Index (SOI), which captures the atmospheric variability, or various indices that describe the oceanic component, such as the sea-surface temperature (SST)-based Nino3.4, or combined indices such as those described by Gergis and Fowler (2005). ENSO and its regional teleconnections are known to vary on interannual, interdecadal, and centennial time-scales (Power et al. 1999a; Diaz et al. 2001; Ault et al. 2013; Brown et al. 2015; Lewis and LeGrande 2015). Over the past 150 years there have been decades with a greater dominance of La Niña

Electronic supplementary material The online version of this article (doi:10.1007/s00382-016-3393-z) contains supplementary material, which is available to authorized users.

✉ Pandora Hope
p.hope@bom.gov.au

[1] Research and Development, Australian Bureau of Meteorology, Melbourne, Australia

[2] ARC Centre of Excellence for Climate System Science, School of Earth Sciences, University of Melbourne, Parkville, Australia

or El Niño events (Power et al. 1999a; Gergis and Fowler 2009), the presence of multi-year persistent events (Allan and D'Arrigo 1999; Cole et al. 2002), and quiescent periods of limited ENSO activity (Kestin et al. 1998).

A good measure of ENSO variability is the power spectrum. The power spectrum of the observed ENSO record has traditionally had the maximum power spectral density (PSD) in the 2–7 years band (Allan et al. 1996). The relative PSD in this band has however varied through the observed record, as measured by the SOI (Kestin et al. 1998). They show that there was greater power in the 1875–1920 C.E. (Common Era, omitted hereafter) time interval, a weakening from 1920 to 1950, and strengthening since 1975 to the end of their record (1995). The dominance of one ENSO phase (El Niño or La Niña) on decadal timescales can create major adaptation challenges (Glantz 2001; Kiem et al. 2003). This time-scale of variability is closely associated with variations in the Interdecadal Pacific Oscillation (IPO) (e.g. Power and Colman 2006). Such variability would be expressed with power in the decadal-to-multidecadal period band of the spectrum.

While the observed record is sufficient to examine ENSO variability on shorter timescales, the record is still less than the estimated 300–500 years needed to capture the full range of unforced ENSO variability (Wittenberg 2009; Bellenger et al. 2014). To gain a better appreciation of any shifts in the spectra of ENSO through time, a range of ENSO series can be used. Firstly, a number of palaeoclimate reconstructions have been developed to help characterise the long-term behaviour of ENSO (Table 1). Further, a range of climate model simulations, which include palaeoclimate simulations of the last 1000 years (850–1850, termed the Last Millennium experiment), have now also become available, run as part of the Coupled Modelling Intercomparison Project Phase 5 (CMIP5) and Palaeoclimate Modelling Intercomparison Project Phase 3 (PMIP3) initiatives (Table 2; Taylor et al. 2012).

Unlike previous studies that characterise past changes in ENSO behaviour solely using climate models (e.g. Ault et al. 2013; Bellenger et al. 2014; Lewis and LeGrande 2015) or palaeoclimate data (e.g. Wilson et al. 2010; McGregor et al. 2013), here we take advantage of available palaeo-ENSO reconstructions and CMIP5–PMIP3 simulations to compare the time-varying nature of ENSO spectra over the Last Millennium from both data sets for the first time. Common changes in the spectral characteristics of ENSO across the models suggest a consistent response to external forcing, while consistent changes across the palaeo-ENSO reconstructions are likely to be the result of external forcing and/or shifts in internal variability.

ENSO variability arises from internal interactions within the climate system, but also includes external forcing from varying greenhouse gases, solar irradiance, and sporadic volcanic eruptions, which all influence the mean state of the global climate (Christensen et al. 2013; Fernández-Donado et al. 2013) and central Pacific (Phipps et al. 2013). Ault et al. (2013) suggest that the variability in the volcanic forcing led to long-term shifts in ENSO behaviour over the Last Millennium; the variability in solar and greenhouse gas forcing was small, and thus was less likely to have played a role in altering the spectra of ENSO.

It should be noted that the different palaeo-ENSO reconstructions and model simulations are not necessarily directly comparable from record to record, but should be internally consistent so that their representation of ENSO in the historical period can be compared with earlier centuries. To estimate the bounds of natural ENSO variability over the Last Millennium we consider the three data sources, each with inherent limitations:

1. Instrumental observations with relatively short record lengths that provide only limited information about low frequency ENSO behaviour, concurrent with non-stationary and uncertain responses to anthropogenic influences;
2. CMIP5–PMIP3 climate model simulations that are imperfect representations of the climate system, are developed using different dynamical parameterisations and have varying estimates of the pre-industrial and anthropogenic transient forcing, and;
3. Palaeoclimate reconstructions that use different ENSO proxies sourced from a range of geographical regions calibrated to a variety of different predictand indices (e.g. SOI, Nino3.4), and with shifts in their variability introduced from data availability and statistical method.

This study aims to determine if there have been past epochs when there were major shifts in the ENSO spectrum, with a particular focus on the decadal band. If these epochs align across the reconstructions and climate models it strongly suggests that they were externally forced.

The study is organised as follows: Sect. 2 describes the instrumental, climate model and palaeoclimate data used in the study, Sect. 3 outlines spectral methods, and the results are presented in Sect. 4. In Sect. 5 the results are discussed and in Sect. 6 conclusions are summarised.

2 Data and models

2.1 Instrumental data, index and season

Instrumental studies have shown differences in ENSO behaviour depending on the ENSO diagnostic selected

Table 1 Summary of palaeo-ENSO reconstructions considered in this study

ENSO reconstruction	Variable	Time span	Palaeoclimate data source	Geographical region
Braganza et al. (2009)	PC1 of palaeoclimate network	AD. 1525–1982	Coral, tree ring and ice core data	Eastern and Western Pacific
Mann et al. (2009)	January–December Niño 3	AD. 500–2006	Coral, tree ring, sediment and ice core data	Niño 3 region extraction from global SST reconstruction
Li et al. (2011)	21-year Running variance of PC1 of palaeoclimate network	AD. 900–2002	First principal component of tree-ring based North America Drought Atlas	North America
Li et al. (2013)	November–January Niño3.4	AD. 1301–2005	A tree-ring network of 2222 chronologies	Asia, New Zealand, and North and South America
McGregor et al. (2013)	PC1 of palaeoclimate network	AD. 1650–1977	Unified ENSO index from previously published palaeoclimate reconstructions	Pacific Ocean
Wilson et al. (2010) teleconnection (TEL)	December–November Niño 3.4	AD. 1540–1998	11 Coral and one ice core record	All tropical areas within 30°S to 30°N outside of the central-eastern Pacific
Emile-Geay et al. (2013a, b)	December–March Niño 3.4	AD. 1150–1995	Coral, tree ring, sediment and ice core data	Indian and Pacific Ocean
Yan et al. (2011)	January–December SOI rainfall proxy	AD. 50–1955	Five lake and marine sediments	Equatorial Pacific
Stahle et al. (1998)	December–February SOI	AD. 1706–1977	North American tree rings, coral and ice core records	Eastern Pacific

(Hanley et al. 2003; Gergis and Fowler 2005). Many of the proxy records considered here are related more closely to the SST-based indices, such as the Nino3.4 SST index (the SST anomaly in the region 5°N–5°S and 170°W–120°W). Thus, we show results for the Nino3.4 index in model simulations, and present results for both Nino3.4 and SOI in instrumental observations.

The SOI, a surface pressure-based index, benefits from a very long instrumental record (Allan et al. 1991; Allan and Ansell 2006). Some variability measured by the SOI is because of underlying trends in the regional relationships in mean sea-level pressure, rather than an indication of ENSO variability (Ropelewski and Jones 1987; Power and Kociuba 2011). Forced off-equatorial trends are projected to have a greater impact on the SOI into the future (Kociuba and Power 2015). Thus, variability in the SOI is not always solely driven by ENSO. The observed monthly Nino3.4 index is calculated from HadISST (Rayner et al. 2003) over the years 1876–2015. The observed monthly SOI values for the period 1876–2015 are from the Australian Bureau of Meteorology, calculated using the Troup method (Troup 1965).

The seasonal progression of a typical El Niño or La Niña commences in austral spring and peaks in amplitude in austral summer (December–February) (Rasmusson and Carpenter 1982; Rasmusson and Wallace 1983; Allan 2000). Thus we use the September to February mean Nino3.4 or SOI to represent ENSO in each year in both the observed and model data. Reconstructions will often also capture this peak signal, but individual sensors within archives of pre-instrumental ENSO variability may incorporate signals outside of their specific target season (Wilson et al. 2010).

2.2 CMIP5–PMIP3 climate model data

Details of the six CMIP5–PMIP3 coupled climate models used in this study are summarised in Table 2. These models all have data from the following experiments: (1) pre-industrial Control simulations, (2) Historical simulations forced with natural and anthropogenic forcing over the 1850–2005 period, and (3) Last Millennium simulations forced by solar and volcanic variability over the years 850–1850 (Schmidt et al. 2011, 2012).

All of the Last Millennium simulations include varying orbital parameters, either from pre-computed tables, or internally calculated following the equations in Berger (1978). CCSM4, MPI-ESM-P and GISS-E2-R also include land-use change in their Last Millennium simulations (Pongratz et al. 2008). The forcing in the Control is fixed as pre-industrial, and does not vary through time. The forcing imposed in the Last Millennium simulations are also given in Table 2. There are known differences in the implementation of solar and volcanic forcing used in models (Table 2),

Table 2 Details of the CMIP5–PMIP3 climate models considered in this study and the forcing applied in their Last Millennium simulations

Climate model	References	Atmospheric resolution	Ocean resolution	Institute	Solar forcing	Volcanic forcing
BCC-CSM1-1	Xin et al. (2013)	128 × 64 × L26	360 × 232 × L40	BCC	Vieira and Solanki (2009) spliced to Wang et al. (2005)	Gao et al. (2008)
CCSM4	Landrum et al. (2013)	288 × 192 × L26	320 × 384 × L60	NCAR	Vieira and Solanki (2009) spliced to Wang et al. (2005)	Gao et al. (2008)
CSIRO-Mk3L-1-2	Phipps et al. (2012)	64 × 56 × L18	128 × 112 × L21	UNSW	Vieira and Solanki (2009) spliced to Wang et al. (2005)	Crowley and Unterman (2013)
GISS-E2-R	Schmidt et al. (2006)	144 × 90 × L40	288 × 180 × L32	NASA GISS	Vieira and Solanki (2009) spliced to Wang et al. (2005)	Crowley and Unterman (2013)
IPSL-CM5A-LR	Hourdin et al. (2013)	182 × 149 × L31	96 × 95 × L39	IPSL	Vieira and Solanki (2009) spliced to Wang et al. (2005)	Ammann et al. (2007)
MIROC-ESM	Watanabe et al. (2011)	128 × 64 × L80	256 × 192 × L44	MIROC	Lean et al. (2005)	Sato et al. (1993)
MPI-ESM-P	Jungclaus et al. (2012)	196 × 98 × L47	256 × 220 × L40	MPI	Vieira and Solanki (2009) spliced to Wang et al. (2005)	Crowley and Unterman (2013)

and varying responses to volcanic forcing (Emile-Geay et al. 2008; McGregor and Timmermann 2011; Zhang et al. 2013), however we consider all models with available Historical, Control and Last Millennium simulations here. As simulations run using the MIROC model (Watanabe et al. 2011; Sueyoshi et al. 2013) are known to display a strong drift over the last 1000 years, they were excluded from further analysis.

We note that the available model simulations were not necessarily continuous from their Last Millennium simulations into their Historical simulations. However, as each model version was the same across the Control, Historical and Last Millennium simulations, the ENSO spectral characteristics should be consistent across the three simulations. Nino3.4 was computed from each model's monthly SST field for the three experiments, and the long-term monthly means from each simulation were removed (i.e. 850–1850 for the Last Millennium and 1851–2005 for the Historical). September to February Nino3.4 values were then averaged.

2.3 Palaeoclimate ENSO reconstructions

There are a number of ENSO reconstructions based on palaeoclimate data that extend centuries before the instrumental period. Detailed discussion of the strengths and weaknesses of some of these techniques is outlined in Gergis et al. (2006) and Wilson et al. (2010). Details of each of the seven published ENSO reconstructions used in this study are summarised in Table 1. The reconstructions are based on a diverse range of annually-resolved tree-ring, coral, ice core and sedimentary records. Note that there are differences in the target predictand used to represent ENSO (e.g. SOI, Nino3.4 SSTs), seasonal window, underlying palaeoclimate data sources and geographical coverage, that all influence the history of ENSO variability inferred by each reconstruction (Table 1). For instance, the Nino3.4 SST reconstruction of Li et al. (2013) only represents the SST component of the coupled system, while reconstructions such as Stahle et al. (1998) use palaeoclimate records from regions with strong ENSO teleconnections to reconstruct the atmospheric component of ENSO represented by the SOI. Some lower-frequency reconstructions of past ENSO do not capture interannual ENSO variability so were not included in this analysis (Mann et al. 2009; Yan et al. 2011).

It should be noted that all ENSO reconstructions contain inherent biases due to differences in underlying palaeoclimate records, data processing and reconstruction methods that impose analytical constraints on the interpretation of our results. For example, all reconstructions based on tree ring measurements suffer from a loss of records back in time, which may influence the reconstructed ENSO variance. Nevertheless, it is common practice in dendrochronology to ensure that a high enough Expressed Population Signal (EPS) and sample replication is present in final 'master chronologies' used for the development of climate reconstructions (Briffa and Jones 1990). In the Nino3.4 SST reconstruction of Emile-Geay et al. (2013a), the reported reduction in variance in the pre-1300 section of the reconstruction is influenced by factors such as

the decreasing availability of predictors back in time, and a lack of coherence at internal timescales due to possible dating errors in the palaeoclimate records. Calibrating palaeoclimate records to observed ENSO variability typically involves many statistical processes including data detrending and variance-adjustments such as pre-whitening (Stahle et al. 1998). These caveats have the potential to influence the time-varying spectra of the series.

Finally, we acknowledge that some of the ENSO reconstructions listed in Table 1 use similar predictors, and thus they are not entirely independent. Accordingly they are not treated as such here. Following the approach of McGregor et al. (2010), we simply make use of all available ENSO reconstructions initially without a priori exclusions, but note that each reconstruction may not be statistically independent of one another.

Many of these studies describe the spectrum of their reconstruction (e.g. Stahle et al. 1998; Braganza et al. 2009). In addition, Braganza et al. (2009) also describe how the ENSO spectrum has varied through time, and aspects of their method are followed here.

3 Methods

3.1 Power spectral density (PSD) and average PSD in frequency bands

This study examines the frequency-domain behaviour of Nino3.4 or palaeo-ENSO reconstructions in: i) power spectral density (PSD) distributions and ii) time-varying band power in the 2–3, 3–8 and 8–25 years frequency bands. Power spectral density (PSD) is computed using the Multi-Taper Method (MTM; Thomson 1982; Percival and Walden 1993; Mann and Lees 1996) with 95% confidence limits computed from a Chi squared distribution. Each power spectrum is compared to that of a lag-one autoregressive (AR1) model with equivalent parameters, with lag-one autocorrelation $\rho_1 = \max(0, r_1)$, where r_1 is the sample autocorrelation.

Band power in the frequency ranges of 2–3, 3–8, 8–25 years is computed by integrating PSD estimates with the rectangle method in 50-year intervals using a 49-year overlap. The total band power is also given. The band power estimate for each window is shown on the central year of the 50-year time window. The Z-scores are calculated to provide an estimate of which peaks are unusually large. The shortest timeseries in this study is 136 years long (the observed ENSO indices), and even with the reduction in the degrees of freedom due to the overlap in the underlying data from one 50 years window to the next, the series are long enough to consider peaks with a Z score >2 to be significant.

Welch's method (Welch 1967) and wavelet analysis are also performed, and the results are similar to those produced using the MTM method described above. As such, only the MTM method has been shown here to facilitate comparison with other studies (e.g. Emile-Geay et al. 2013b).

4 Results

4.1 ENSO statistics from observations, reconstructions and models

The timeseries of the observed September to February Nino3.4 and the annually-resolved ENSO reconstructions are presented in Fig. 1. The climate models' September to February Nino3.4 timeseries are displayed in Fig. 2, with the results from the Historical simulation concatenated to those from the Last Millennium simulations. The palaeo-ENSO reconstructions in Fig. 1 all display interannual variability of a magnitude that might be considered to represent observed ENSO variability.

Although climate models would not be expected to capture the exact timing of ENSO events, we would expect that they represent the statistical characteristics of the observed record during the historical period. The timeseries of simulated Nino3.4 are shown in Fig. 2, and comparison can be made between the models. The BCC-CSM-1 model displays higher frequency Nino3.4 variations than models such as CSIRO-Mk3L-1-2 and MPI-ESM-P. Higher Nino3.4 amplitude is present in the CCSM4, MPI-ESM-P and BCC-CSM1.1 simulations than in the CSIRO-Mk3L-1-2 and GISS-E2-R models.

The variability and structure of each ENSO timeseries post-1850 is assessed using basic statistical metrics (Tables 3, 4). The observed Nino3.4 has a standard deviation of 1.14 °C and a slightly skewed probability density function (PDF), with a positive skewness of 0.36. The kurtosis measure is as expected from a normal distribution, close to three (2.89). There is an insignificant lag-one autocorrelation (−0.03) and a negative autocorrelation at the two-year lag (−0.23). Statistics of the Historical modelled Nino3.4 series (1850–2005) are shown in Table 3. The standard deviation of Nino3.4 in the CCSM4 model (1.28) is slightly greater than observed; all other models have lower variance (the standard deviation range is 0.65–0.80). The likelihood of extremes (e.g. strong La Niña or El Niño events) through the historical period can be characterised by the skewness and kurtosis; all the models except MPI-ESM-P have a kurtosis similar to observed, suggesting a near-normal distribution. The higher value for MPI-ESM-P means its distribution is peaked relative to a normal distribution, with a stronger tendency for values near the mean

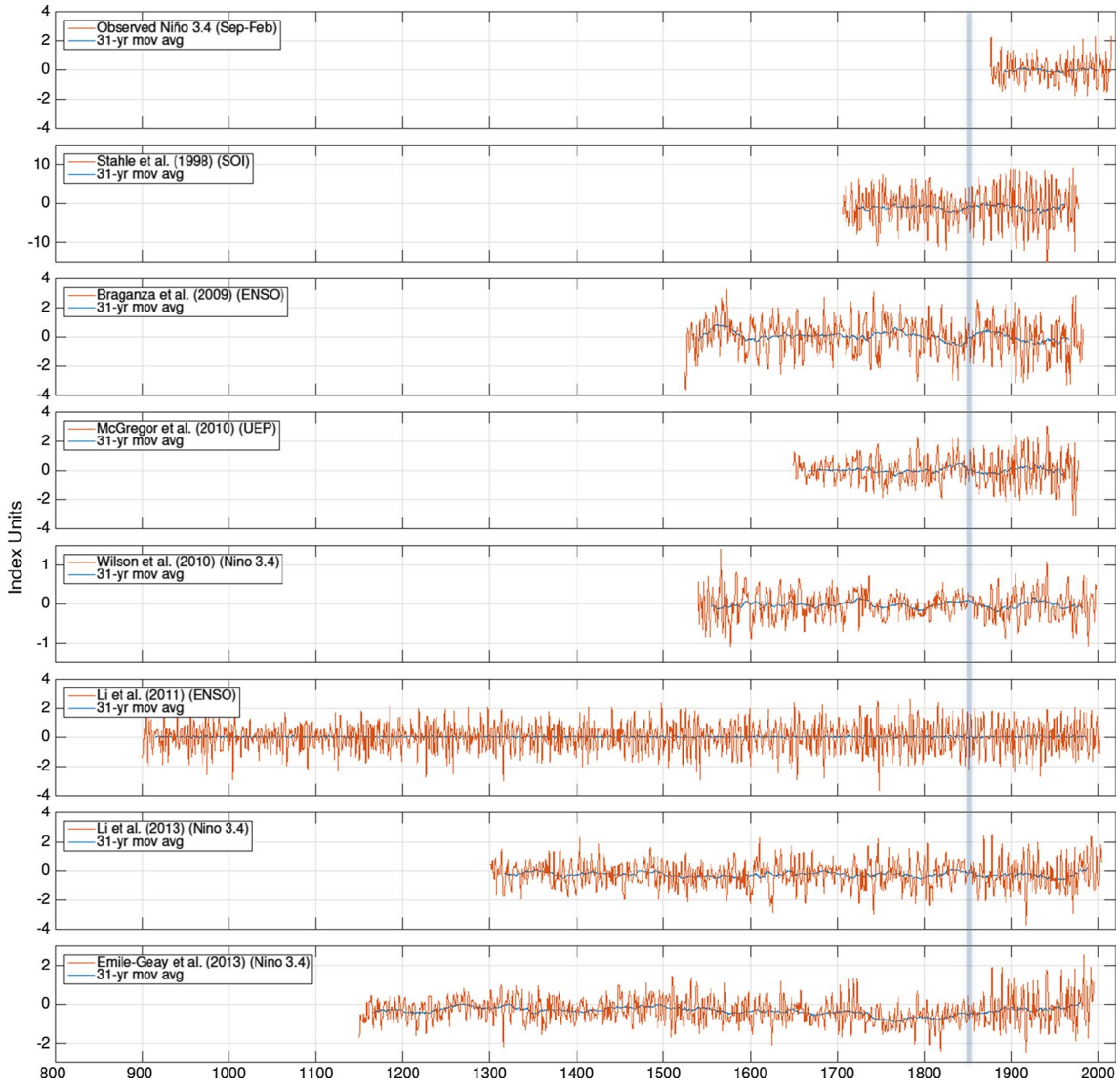

Fig. 1 Time series of annual (*red*) and 31-year smoothed (*blue*) Nino3.4 in instrumental data (*panel 1*) and ENSO palaeoclimate reconstructions (*panels 2–8*) in chronological order of publication. *Grey vertical line* at 1850 delineates pre-industrial from the historical period

(Fig. 2), fewer moderate deviations and a higher chance of extremes well beyond the mean.

The statistical metrics for each ENSO reconstruction over the post-1850 period are summarised in Table 4. The standard deviation is in the units of the reconstructed ENSO index and thus reconstructions of Nino3.4 can be directly compared with the observed value in Table 3. The Stahle et al. (1998) reconstruction is comparable to the SOI, for which the observed series has a standard deviation of 8.22. For those series that can be compared with observations, the variability of the reconstructions is lower than observed.

Note that reconstructions that reflect surface temperature will also include a contribution from global warming in recent decades. This is less evident in the reconstructions that use the leading principal component of palaeoclimate data variability as an uncalibrated 'ENSO index' (e.g. Braganza et al. 2009; McGregor et al. 2010). The Stahle et al. (1998), Li et al. (2013) and Emile-Geay et al. (2013a, b) series exhibit a weak negative autocorrelation at lag-two, similar to observed Nino3.4. The Wilson et al. (2010) record shows relatively strong positive autocorrelation at lag one, possibly due to tree ring standardisation techniques designed to retain low frequency variations. Overall, the ENSO reconstructions broadly reflect features of the observed series, particularly with respect to the negative autocorrelations at a lag of two years. With regards to autocorrelation at lags one and two, the reconstructions of Stahle et al. (1998) (0.01, −0.29) and Emile-Geay et al.

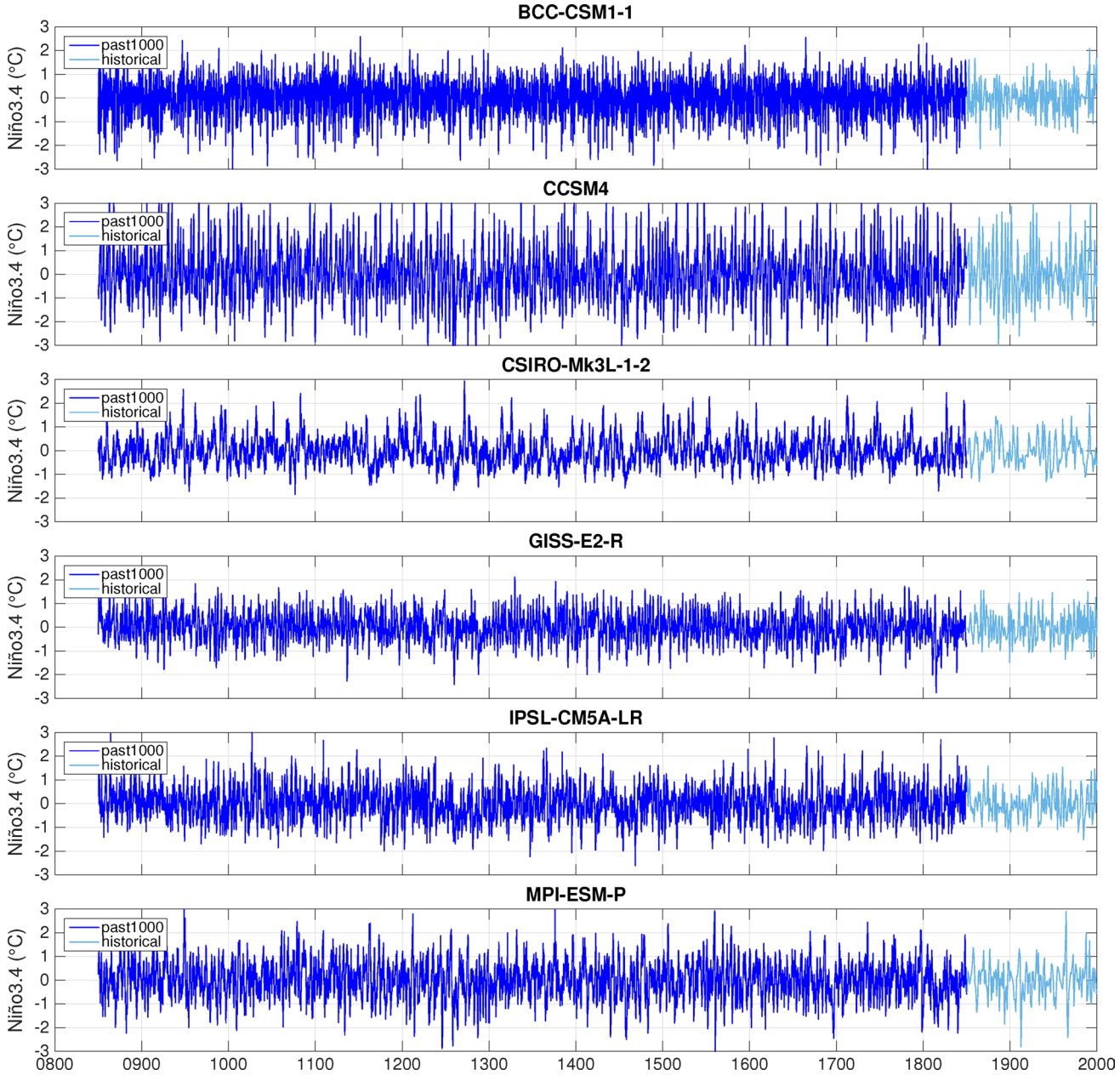

Fig. 2 Time series of CMIP5–PMIP3 modelled September–February Nino3.4 over the Last Millennium (850–1850, *dark blue*) and Historical (1851–2005, *light blue*) simulations. The long-term monthly means were removed from each Nino3.4 series before the calculation of the September–February average

Table 3 Key statistics of September–February Nino3.4 in observations (1870–2005) and CMIP5–PMIP3 models Historical (1850–2005) experiments (°C)

	Observed	BCC-CSM1-1	CCSM4	CSIRO-Mk3L-1-2	GISS-E2-R	IPSL-CM5A-LR	MPI-ESM-P
Mean	0.00	0.00	0.00	0.00	0.00	0.00	0.00
Stdev	1.14	0.80	1.28	0.65	0.68	0.66	0.78
Skewness	0.36	−0.04	0.37	0.35	0.25	0.26	−0.17
Kurtosis	2.89	2.69	2.84	2.77	2.45	2.49	4.66
Lag-one autocorrelation	−0.03	−0.53	−0.07	0.41	−0.25	−0.02	0.12
Lag-two autocorrelation	−0.23	0.24	−0.48	0.03	−0.16	−0.07	−0.19

Table 4 Key statistics of post 1850 characteristics of the palaeo-ENSO reconstructions listed in Table 1

	Stahle et al. (1998) (SOI)'	Braganza et al. (2009) (ENSO)'	McGregor et al. (2010) (UEP)'	Wilson et al. (2010) (Nino3.4)'	Li et al. (2011) (ENSO)'	Li et al. (2013) (Nino3.4)'	Emile-Geay et al. (2013a, b) (Nino3.4)'
Mean	−0.93	−0.08	−0.04	−0.04	0.00	−0.27	−0.22
Stdev	5.52	1.35	1.24	0.39	1.11	1.11	0.93
Skewness	−0.20	−0.30	0.12	−0.03	−0.16	0.25	0.50
Kurtosis	2.50	2.70	2.63	2.85	2.22	3.13	2.93
Lag-one auto-correlation	0.01	0.15	0.11	0.40	−0.18	0.16	0.03
Lag-two auto-correlation	−0.29	0.03	−0.09	−0.08	−0.29	−0.19	−0.17

(2013a, b) (0.03, −0.17) agree best with the observed Nino3.4 values (−0.03, −0.23).

Quantile–quantile plots of modelled and observed Nino3.4 (Supp. Figure S1) provide further information about the behaviour of the tails of the distributions, and show that the intensity of El Niño or La Niña are weaker compared to the observed record in every model except CCSM4, where extreme ENSO events tend to be simulated with higher amplitude than in observed data. However overall, the CCSM4 simulated Nino3.4 distribution matches the observed record better than the other models.

Most of the models have autocorrelation structures that do not match particularly well with the observed Nino3.4. For example, BCC-CSM-1 has a strong negative lag-one autocorrelation (−0.53), followed by a strong positive lag-two autocorrelation (0.24) indicating a tendency to switch ENSO phase from year to year (a strong biennial cycle) and CSIRO-Mk3L-1-2 has high interannual persistence, with a strong positive correlation at lag one (0.41).

The climate models vary in their representation of the time-variation and magnitude of Nino3.4 under Historical forcing compared to the observed, with different strengths and weaknesses. Aspects such as the strong biennial nature of BCC-CSM-1, the high kurtosis of MPI-ESM-P, and the lower amplitude of modelled Nino3.4 relative to observed in all models except CCSM4, all contribute to the signature of each models' Nino3.4 frequency spectrum. With this in mind, we next examine the full power spectrum of September to February Nino3.4 from these models and assess whether their spectra are different under external forcing by comparing the Last Millennium simulations to the pre-industrial Control simulations.

4.2 Power spectra of ENSO indices

The power spectra of the instrumental Nino3.4 (Fig. 3) has the well documented ENSO peaks in the 2–7 years frequency band (e.g. Allan et al. 1996). The SOI spectrum is also shown for comparison in Fig. 3, and exhibits similar peaks.

The power spectra for each palaeo-ENSO reconstruction is shown in Fig. 4. To allow for comparison with observational and model data, the reconstructions are analysed separately for the pre and post-1850 period. The post-1850 power spectra of Stahle et al. (1998), Wilson et al. (2010), Li et al. (2011) have significant power above the red-noise line in the same range as the observed spectrum. The Li et al. (2013) and Emile-Geay et al. (2013a, b) reconstructions also have similar spectra to that of the observed, but with weaker power density in the 2–3 years period band. The spectra of the Braganza et al. (2009) and McGregor et al. (2010), and to some extent the Wilson et al. (2010) reconstructions, are close to the red noise line. At longer periods, the power density is significant at about 10 years in the Braganza et al. (2009) spectrum. Others either follow the red-noise curve, or power diminishes at a rate similar to in the observations, except for the spectrum of the Li et al. (2011) reconstruction of variance, which appears to have little power at longer periods.

The spectra based on the pre-1850 reconstructions (Fig. 4) have more frequency detail than the post-1850 spectra due to the longer data records prior to 1850. All have similar features to their post-1850 counterparts, for instance, Li et al. (2011) has the same strong power around 3–8 years that then attenuates quickly at longer periods, and both the pre- and post-1850 spectra of Braganza et al. (2009) have a peak at around 10 years. The spectra from the pre-1850 section of the Wilson et al. (2010) reconstruction has a strong peak at 10–18 years that is not evident in the post-1850 spectra, suggesting strong decadal variability through the early part of the record, as noted by McGregor et al. (2013). However, there are a various aspects of the development of the reconstructions that could influence lower frequency variability further back in time, including the nature of the data, statistical methods and dating uncertainties (Bradley 1996).

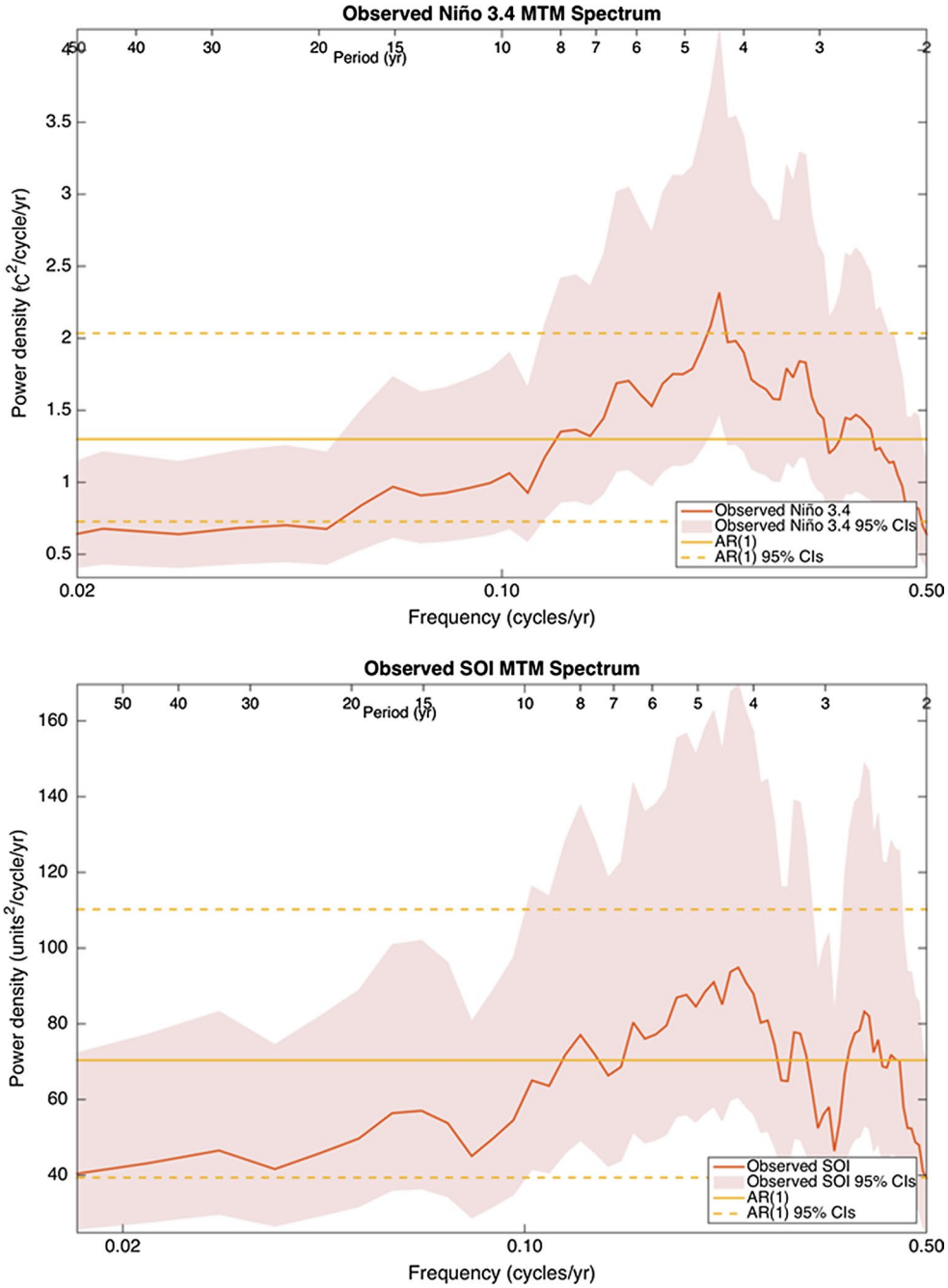

Fig. 3 Observed power spectrum of instrumental data for September–February Nino3.4 (*top panel*) and SOI (*lower panel*) indices. The *solid orange line* denotes the *red* noise level, with 95% confidence intervals *dotted*

Figure 5 shows the power spectra of Nino3.4 from the Historical (1850–2005) simulations from six CMIP5–PMIP3 models. We expect models to represent the statistical nature of the observations, but not the observed timing, unless the model is responding to external forcing common to both observations and the forcing applied in the model simulations. There are substantial differences between the models. For example, the BCC-CSM-1-1 spectrum is dominated by biennial periodicity, whereas the MPI-ESM-P, CCSM4 and CSIRO-Mk3L-1-2 models show little periodic behaviour above red noise on timescales shorter than 3 years.

Of the models analysed here, CCSM4 displays spectral peaks most closely aligned with the 2–7 years peaks present in the instrumental Nino3.4 (Fig. 3). Three of the models (BCC-CSM-1-1, GISS-E2-R, and CCSM4) have little power at periodicities greater than 10 years, while the observed series have evidence of lower frequencies at decadal to interdecadal timescales. Conversely, the CSIRO-Mk3L-1-2 and MPI-ESM-P models have strong broad

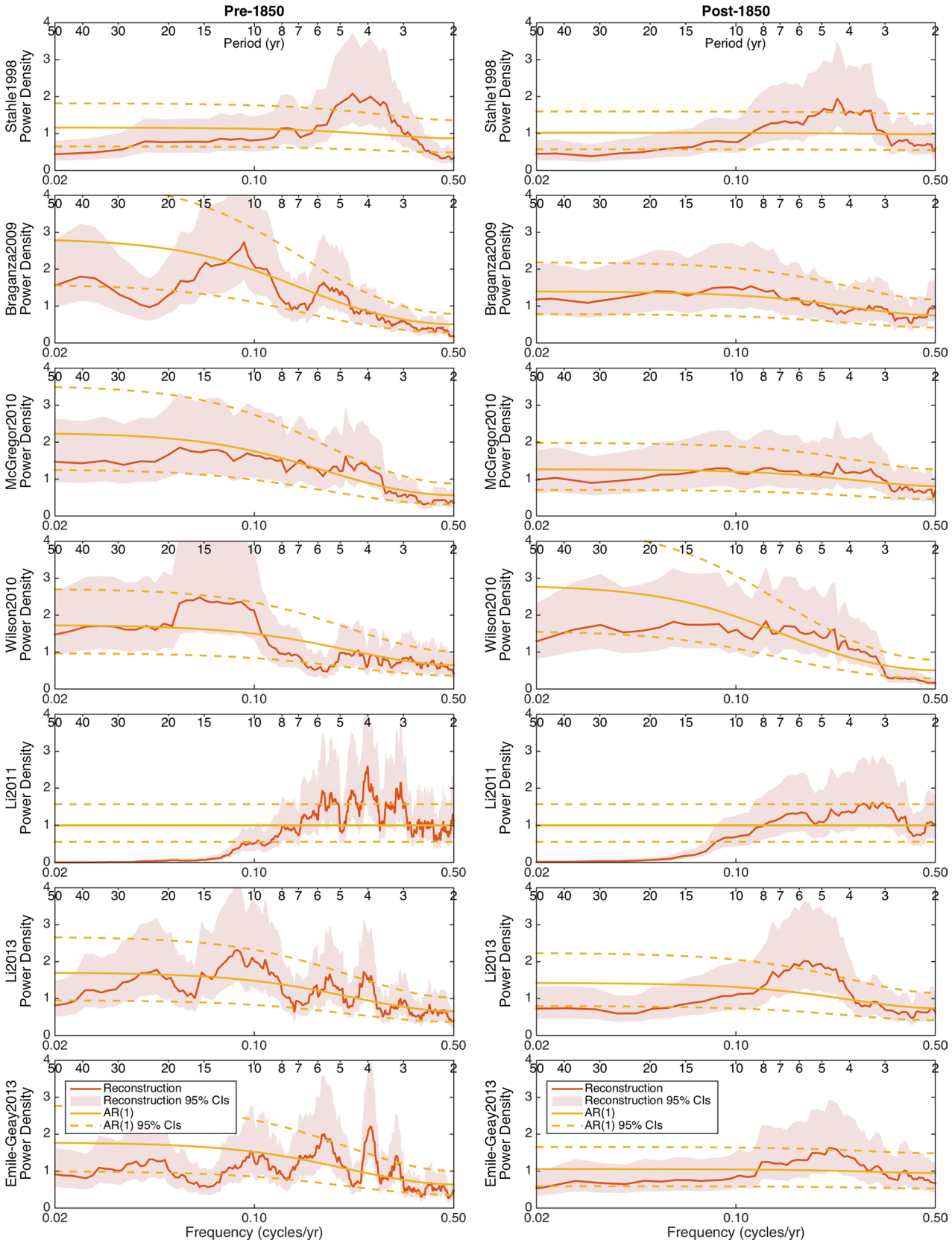

Fig. 4 Power spectral density over pre-1850 (*left column*) and post-1850 (*right column*) years for each paleoclimate ENSO reconstructions. The *solid orange line* denotes the red noise level, with 95% confidence intervals *dotted*

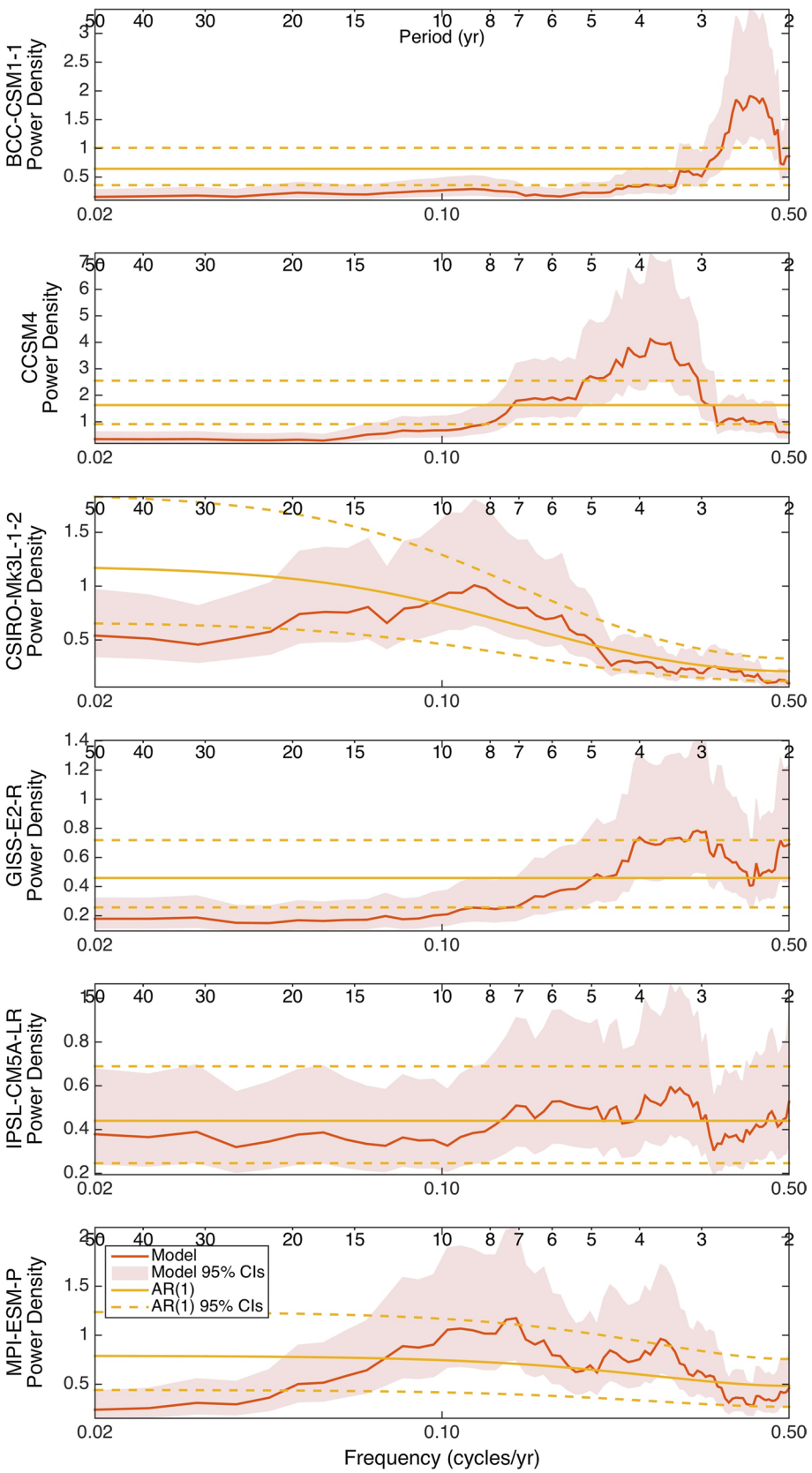

Fig. 5 Power spectral density for CMIP5–PMIP3 Historical simulations (1851–2005). The *solid orange line* denotes the *red* noise level, with 95% confidence intervals *dotted*

peaks at decadal-scale periods (7–10 years). These differences in spectra highlight strong intrinsic differences in the model representations of the frequency behaviour of ENSO. The Nino3.4 spectra of the GISS-ER-2, CCSM4 and IPSL-CM5A-LR models better represent the spectrum of the observed Nino3.4 than the other models considered in this study.

The spectral characteristics of Nino3.4 from the Last Millennium experiments over the 850–1850 period and the pre-industrial Control simulations are shown in Fig. 6. The Control and Last Millennium spectra have similar characteristics to their Historical spectra, although with higher frequency detail. The spectra of the MPI-ESM-P simulations have greater power at longer periods than in that model's Historical simulation. The significant peak is broader in the Last Millennium Nino3.4 spectrum from CCSM4 than in the Historical, and both are broader than the narrow band in the Control, suggesting that different forcing in the Last Millennium and Historical simulations generate a wider range of ENSO behaviour in the frequency domain. For the other models analysed here, there is no strong indication of a consistent broadening of the peaks in the Last Millennium spectrum compared to the Control.

4.3 Temporal shifts in ENSO power spectra over the Last Millennium

To evaluate changes in the nature of ENSO spectra over time, and any changes in the dominance of high and low frequency characteristics, we examine the spectral power in the 2–3 years (near biennial), 3–8 years (classical ENSO) and 8–25 years (decadal) periodicity bands using a 50-year moving window for the instrumental and modelled Nino3.4 and the palaeo-ENSO reconstructions.

Figure 7 shows the three bands for the instrumental Nino3.4 and SOI. Power in the 3–8 years band is generally higher than the other bands, with a greater contribution from the 2–3 and 8–25 years bands early in the record (Figure S2) and the 2–3 years band in most recent years of the Nino3.4 record. For the SOI, the 3–8 years band dominates (Figure S2), until the most recent years, when the PSD in the 2–3 years band is greater, and the 8–25 years band PSD also increases, while the variability on a 3–8 years timescale reduces.

There is a trend towards higher total PSD in the second half of the 20th century in both Nino3.4 and SOI (see also Figure S2). The increase in PSD in the 2–3 and 8–25 years bands rises significantly for the SOI, while for Nino3.4 the rise is driven by variance in the 2–3 and 3–8 years bands. Together, this is reflected in the last 50 years having the highest variability in the record (e.g. Borlace et al. 2013).

Similar to features seen in the observational Nino3.4 and SOI records, a number of the climate models simulate the relative dominance of the 3–8 years frequency band in the moving Nino3.4 spectra from the Historical simulations (CCSM4, CSIRO-Mk3L-1-2, IPSL-CM5A-LR and MPI-SM-P, Fig. 8). The CCSM4 model simulates a balance between Nino3.4 frequency bands that is most similar to the observations pre-1950, although the total PSD is stronger. The relative rise in PSD in the 2–3 years band in recent years is only present in the GISS-E2-R and BCC-CSM1-1 simulations, and only the CSIRO-Mk3L-1-2 spectrum has greater dominance in the decadal band over the 3–8 years band in recent years. Although the change is small, the power in the 8–25 years band of the Nino3.4 spectrum of CCSM4 rises significantly in recent years compared to previous power in this band in this model (Figure S3).

Three of the models (CCSM4, GISS-E2-R and BCC-CSM1-1) have significant peaks in PSD in at least one period band at the end of the record. Given the wide range of characteristics in ENSO spectra shown by the individual models and uncertainties in the ENSO response to increasing greenhouse gas forcing (Vecchi and Wittenberg 2010), the model responses to greenhouse gas forcing might differ (Flato et al. 2013). However, the agreement across these three models suggest some consistent response to external forcing in recent decades.

Figure 9 presents the time-varying PSD in 50 years moving windows for the pre-industrial Control simulations with constant forcing spanning between 450 and 1100 years length of simulation. The power in the three period bands reflects the dominant peaks in the full spectra shown in Fig. 6. The power in the 3–8 years band dominates in the CCSM4, CSIRO-Mk3L-1-2, IPSL-CM5A-LR and MPI-SM-P models' Nino3.4 spectra. The biennial band is most dominant in BCC-CSM1-1 Nino3.4, and the decadal band is dominant in CSIRO-Mk3L-1-2. There are epochs when the greatest PSD shifts from the 3–8 years band to another timescale in CSIRO-Mk3L-1-2 and GISS-E2-R Control simulations, in a similar manner to the observed shift at the end of the twentieth century (for SOI). This supports the idea that observed shifts in the spectral balance are within the range of internal variability as simulated by models. In the CCSM4 model spectrum the 3–8 years band is always dominant, while the decadal band has little power relative to the 3–8 years band, possibly due to the known weakness of the link between the tropics and extratropics in the Pacific in this model (Deser et al. 2011).

The forced Last Millennium simulations show similar time-varying PSD behaviour to the Control runs across all models (Fig. 10). The 3–8 years band dominates in CCSM4, CSIRO-Mk3L-1-2, IPSL-CM5A-LR and MPI-ESM-P, with small multicentennial fluctuations in the relative strengths of the bands. The major volcanic eruptions around 1258, 1452 and 1815 are marked in Fig. 10 and there is a suggestion of changes to the relative balance of

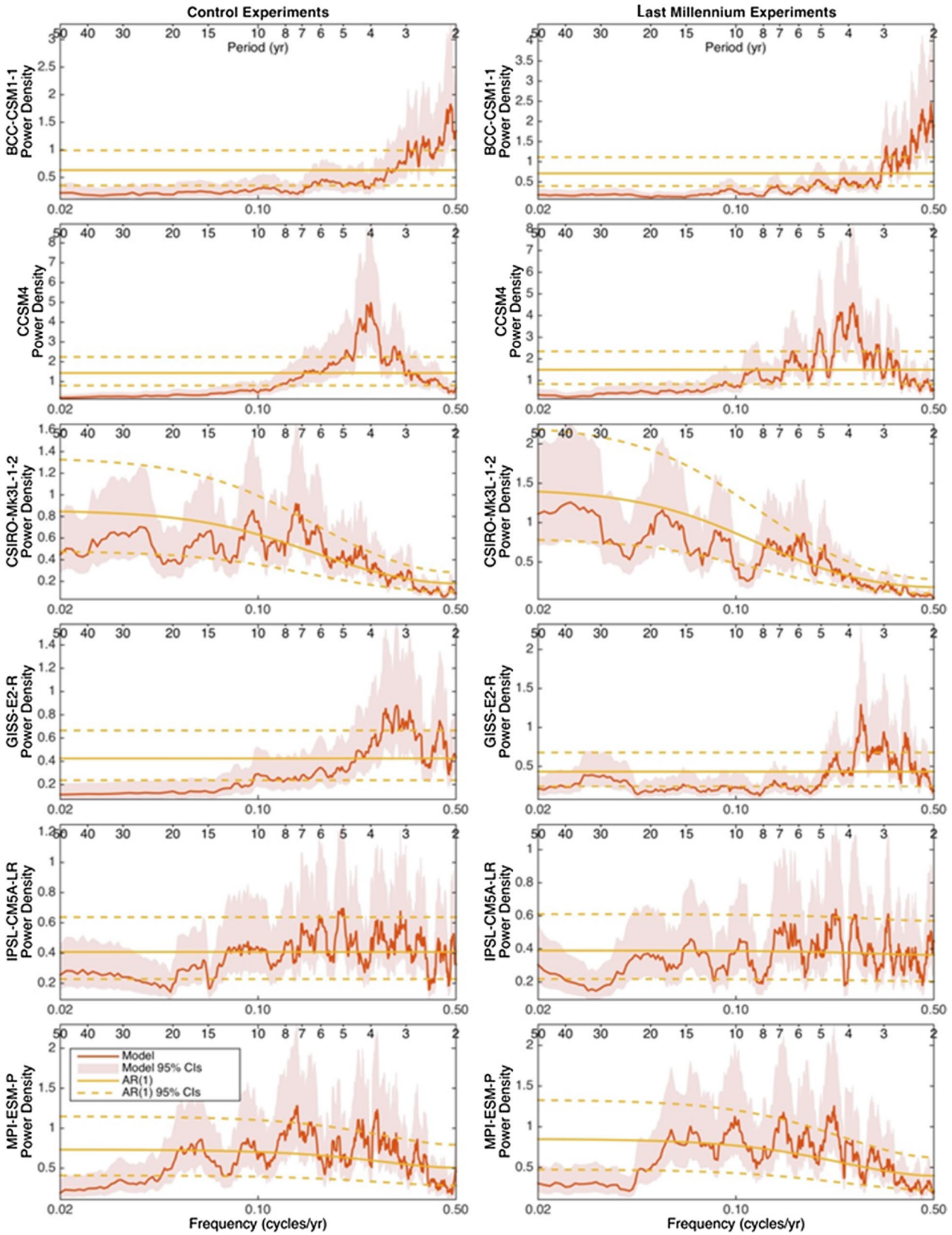

Fig. 6 As Fig. 5, but the power spectral density for Control CMIP5–PMIP3 modelled Nino3.4 (*left column*) and Last Millennium simulations (850–1850) (*right column*)

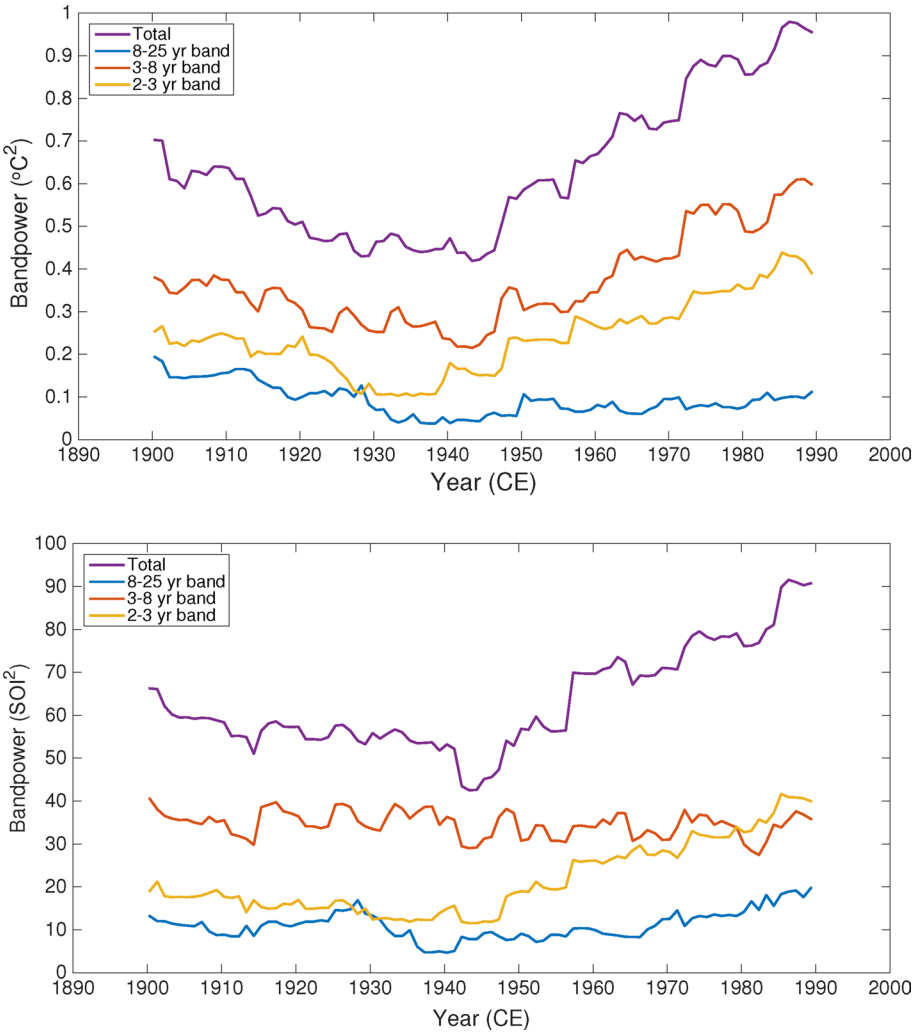

Fig. 7 Timeseries of band-power in several frequency bands in 50-year moving windows from the observed Nino3.4 (*top panel*) and SOI (*lower panel*). The 2–3 (*yellow*), 3–8 (*red*) and 8–25 (*blue*) year bands are shown, with the total spectral power in *purple*

the power spectra around these times, however this is not consistent across models. There is a statistically significant increase in power in the 8–25 years band around the time of the 1258 and 1452 volcanoes in CCSM4, BCC-CSM1-1, GISS-E2-R and MPI-ESM-P (Figure S4). In all models there are other epochs with similarly increased total PSD. A shift might have been expected around the times of volcanic eruptions as there is an extended downward swing in Nino3.4 after these events and evidence of changes in total ENSO variance following these events, seen in the smoothed Nino3.4 series of Brown et al. (2015) and Lewis and LeGrande (2015). The 30-year running variance of all the models except CSIRO-Mk3L-1-2 increased at around the time of the 1815 Tambora volcano (Brown et al. 2015). There is generally a local upturn in 50-year windowed total PSD at that time, but aside from GISS-E2-R, these increases in PSD are not outside the fluctuations seen earlier in the simulation.

The spectral densities in three bins in moving 50-year timeslices for the palaeo-ENSO reconstructions are shown in Fig. 11. The palaeo-ENSO reconstruction timeseries presented in Fig. 1, together with the results in Fig. 11, indicate epochs of significantly higher and lower ENSO variability. For example, the Wilson et al. (2010) record has higher variability early and late in the record, with less variance in 1700–1850, reflected by increased total PSD at the beginning and end of the record. Another example is the increasing variance evident in the McGregor et al. (2010) reconstruction (Fig. 1), seen as increasing total PSD through time in Fig. 11.

The ENSO reconstructions display a relative dominance of spectral power in the 3–8 years band. The Braganza et al. (2009), McGregor et al. (2010) and Li et al. (2013) reconstructions all show a peak in relative power in the 8–25 years band in the early 1700s (see also Figure S5). Further back in time, the Braganza et al. (2009) and Li et al. (2013) reconstructions also show a peak in the decadal band around 1600, suggesting that the reconstructions are capturing a period of ENSO frequency change.

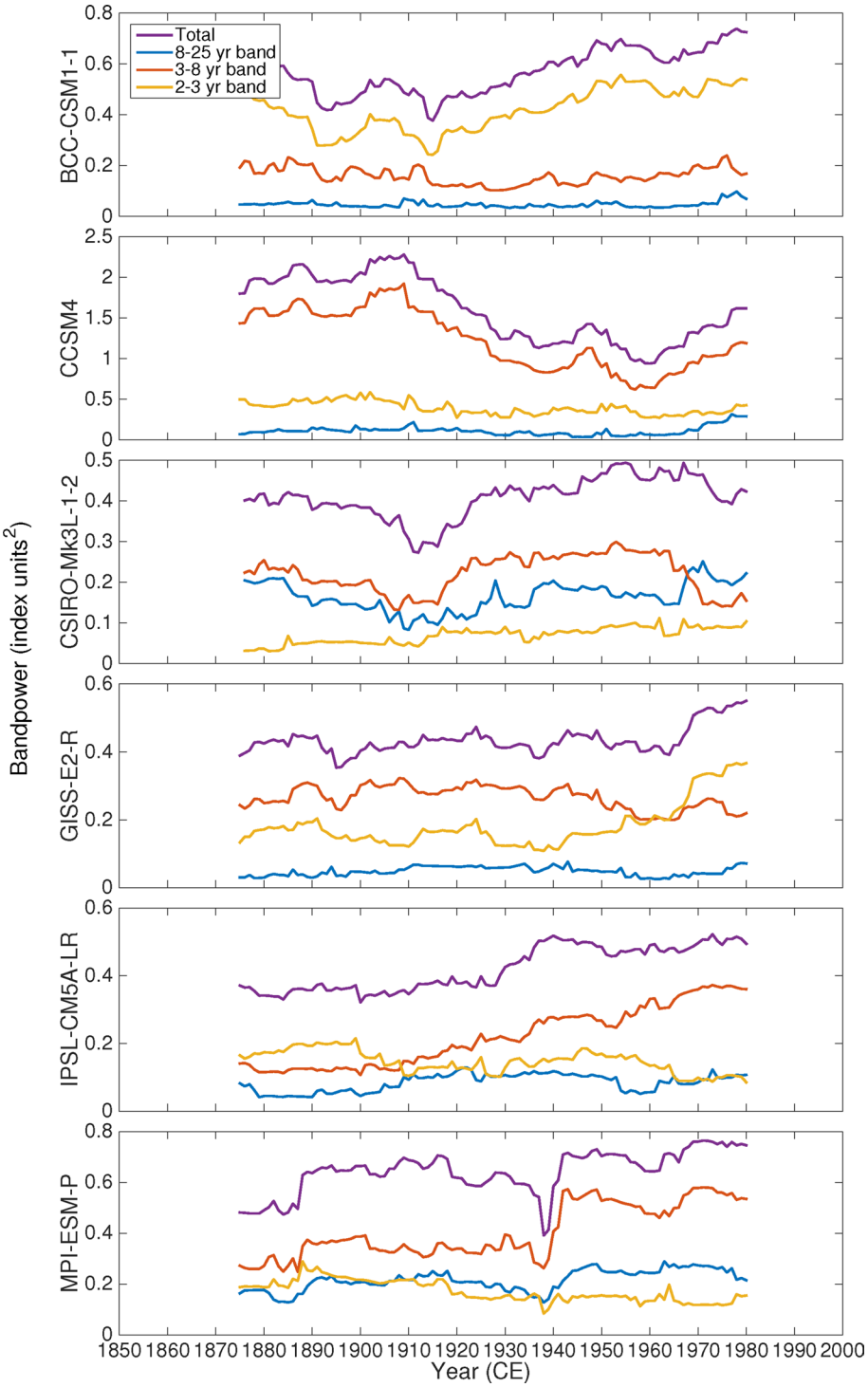

Fig. 8 As Fig. 7, but for Nino3.4 from the CMIP5–PMIP3 Historical experiments

The PSD in all bands increases strongly from the mid-nineteenth century in the Braganza et al. (2009), Emile-Geay et al. (2013a, b), Li et al. (2013), McGregor et al. (2010) and Stahle et al. (1998) reconstructions (Figs. 11 and S5). The moving spectra from the climate model Historical simulations (Fig. 8) show a similar period of high PSD through this same time period in one of the more reliable climate models CCSM4, and significant peaks in the 2–3 years band in the Nino3.4 spectra from the IPSL-CM5A-LR and MPI-ESM-P models (Figure S2).

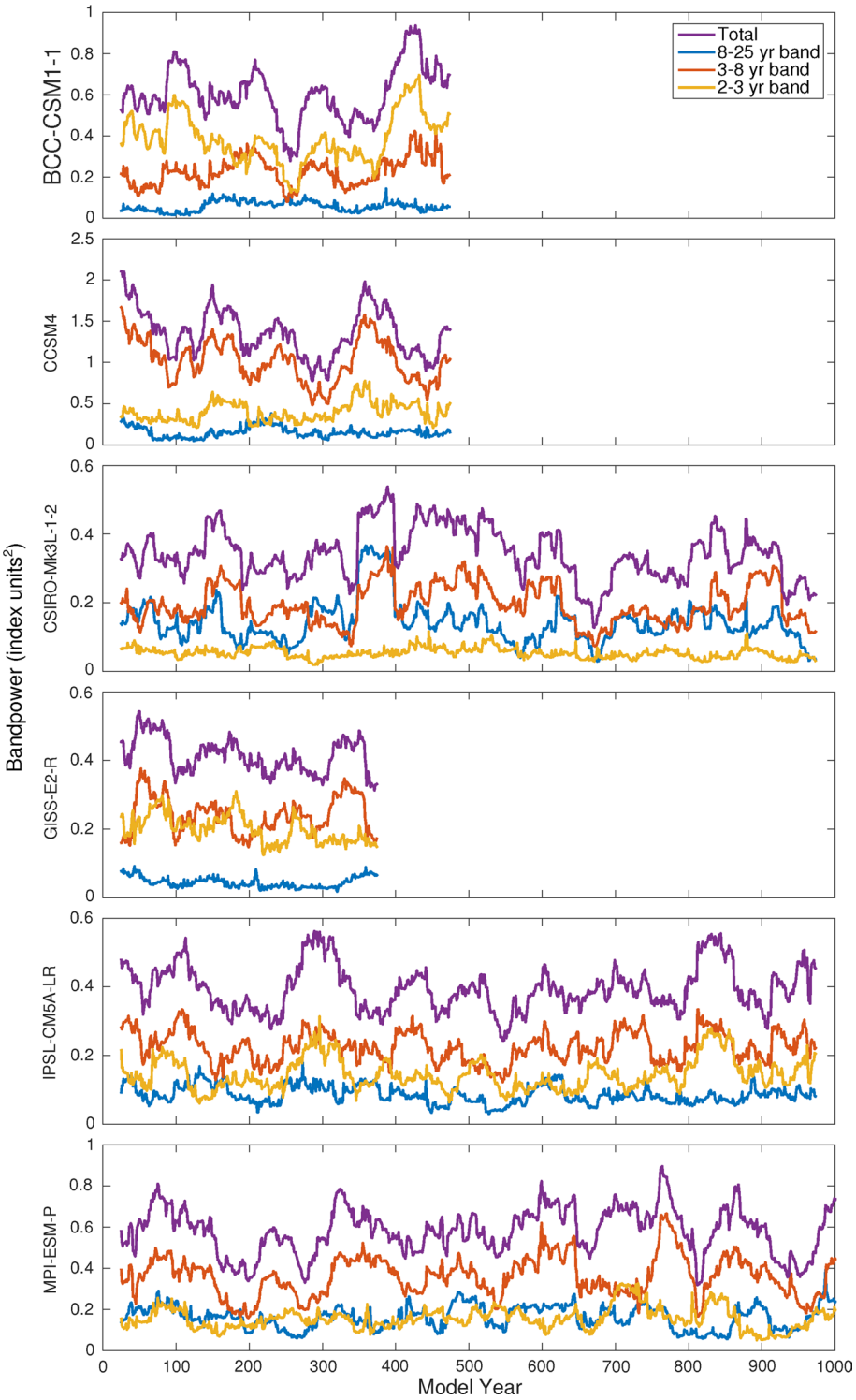

Fig. 9 As Fig. 7, but for Nino3.4 from the CMIP5–PMIP3 pre-industrial Control experiments. The forcing is fixed, and the timescale reflects the length of the simulations

5 Discussion

The spectra of the CMIP5 climate models have been found to vary from model to model. Bellenger et al. (2014) provide an analysis of the representation of ENSO spectra in pre-industrial Control simulations across a large number of CMIP3 and CMIP5 models. The ENSO spectra are not consistent across the range of models. They assessed the ratio of the power in the 1–3 and 3–8 years bands from the ENSO spectra of these models and observations (HadISST1.1). The observations have power in both bands, with slightly more variance in the 3–8 years band. Earlier

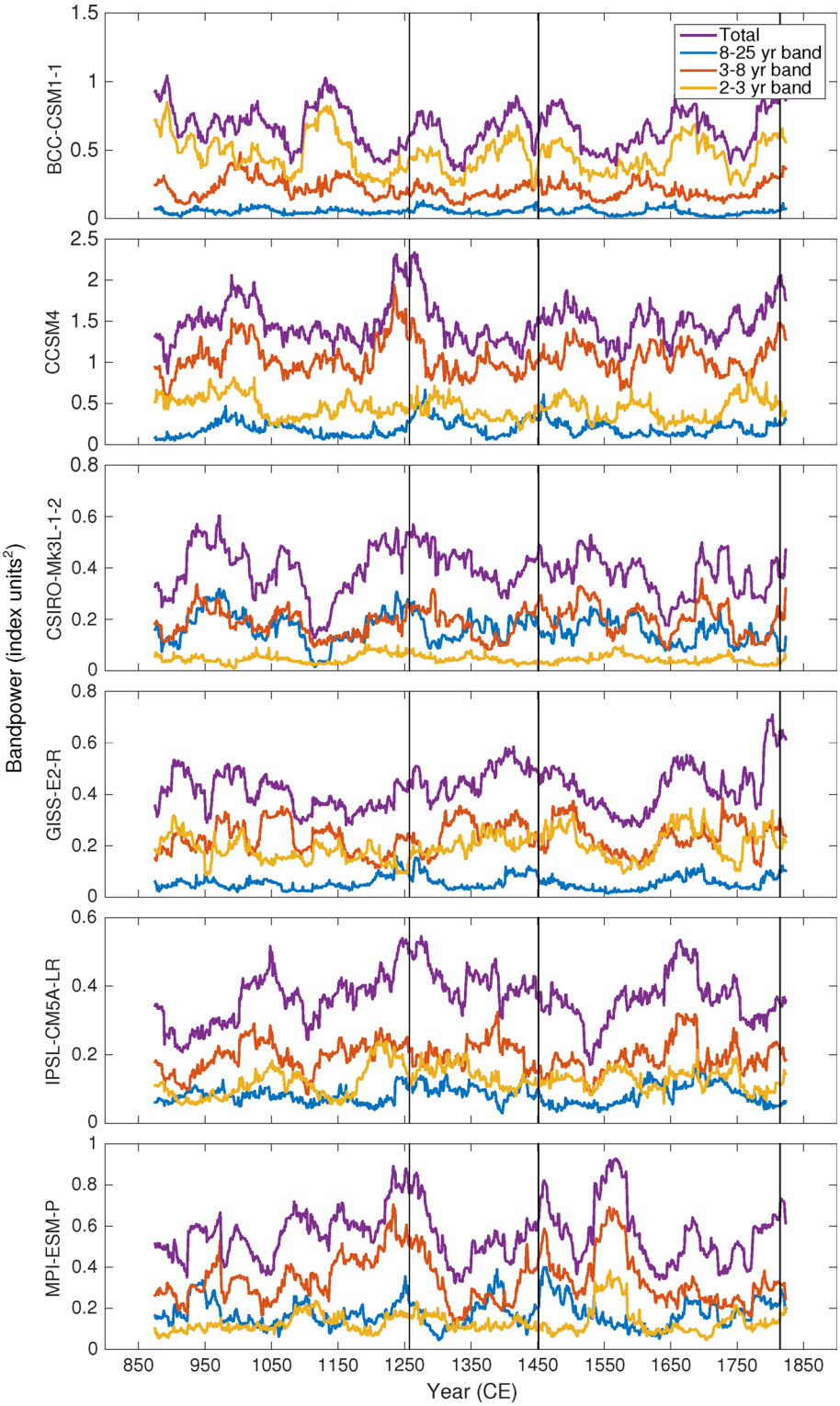

Fig. 10 As Fig. 7, but for Nino3.4 from the CMIP5–PMIP3 Last Millennium (850–1850) experiments. *Vertical lines* indicate the timing of major volcanic eruptions

work (Wittenberg et al. 2006) found that the BCC-CSM1 model simulates ENSO with too short a period, although other models (e.g. CCSM4) exhibit characteristics similar to instrumental observations. The more recent CMIP5 versions of models tend to have more power at longer periods than earlier (CMIP3) versions that often had little power at periods greater than three years (Wittenberg et al. 2006).

The climate models assessed here also display considerable inter-model differences in ENSO characteristics such as frequency and variance. However, the spectral

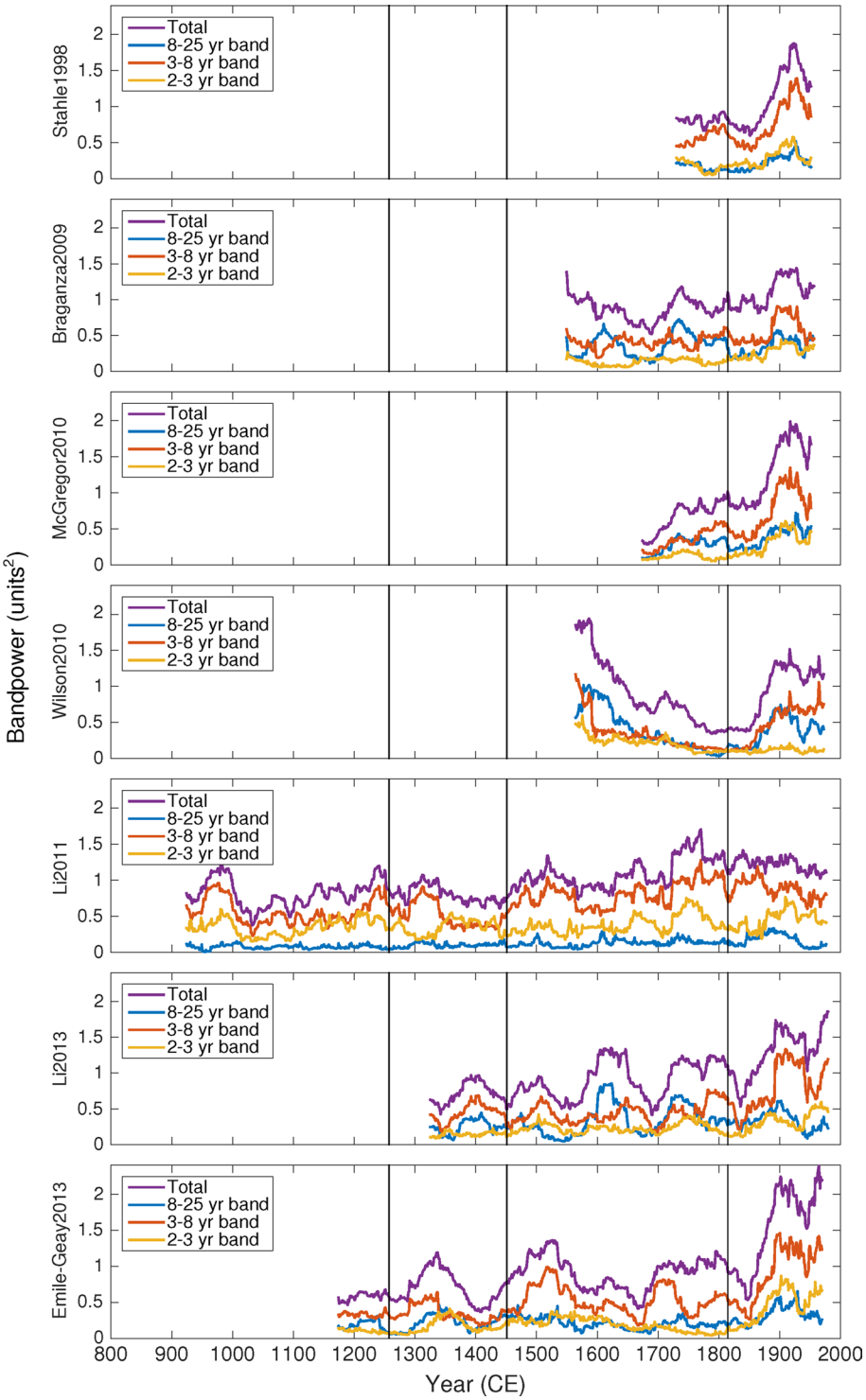

Fig. 11 As Fig. 7, but for the palaeo-ENSO reconstructions. *Vertical lines* indicate the timing of major volcanic eruptions

characteristics of ENSO across the Historical, Last Millennium and pre-industrial Control simulations from each individual model are largely consistent, confirming that internal variability is the major driver of ENSO variability rather than external forcing.

Earlier studies have shown that external forcing in climate models (for instance, volcanoes in the Last Millennium, as well as changes to atmospheric composition in the Historical period) result in a wider range of frequency behaviour compared to the pre-industrial Control (Ault et al. 2013; Emile-Geay et al. 2013a, b; Landrum et al. 2013). In this study we find that this is the case for CCSM4, the model used by Landrum et al. (2013) and Emile-Geay et al. (2013a, b). This increased power at

lower frequency in the Last Millennium simulations, however, is evident in only one model. Thus, for the other four CMIP5–PMIP3 models considered here, ENSO represents an inherent mode of internal climate variability with spectral characteristics that are not strongly influenced by external forcing in the Last Millennium. However, despite this, models show a consistent multi-decadal response after the major volcanoes over the Last Millennium (Brown et al. 2015; Lewis and LeGrande 2015). This study provides evidence for an increase in spectral power in four models, particularly in the decadal band, around the time of the major 1258 and 1452 volcanic eruptions.

Many studies have explored the influence of volcanic eruptions on the behaviour of ENSO (Nicholls 1988; Adams et al. 2003; Emile-Geay et al. 2008; McGregor and Timmermann 2011; Zhang et al. 2013; Stevenson et al. 2016). Using a range of palaeoclimate records, Adams et al. (2003) suggest the predominance of El Niño-like conditions after major volcanic events. The work of Emile-Geay et al. (2008) supports this finding for very large volcanic eruptions, noting that the eruption does not create the event, but enhances the likelihood of an El Niño. These findings are also supported by studies with the coupled climate model MIROC5i (Ohba et al. 2013), where it is believed the widespread tropical cooling acts to cool the western Pacific more than the east, enhancing El Niño-like conditions. Stevenson et al. (2016) found the ENSO response to volcanic eruptions varied with the hemisphere of eruption in the CESM Last Millennium ensemble. However, in the CCSM3 model, the immediate ENSO response after a major volcanic eruption was reported by McGregor and Timmermann (2011) to be more La Niña-like.

The longer-term response was found by Brown et al. (2015) and Lewis and LeGrande (2015) to be La Nina-like, shown with multi-decadal running-mean values of Nino3.4 in the years following the 1258 eruption across the models examined here. Although some studies have found a decadal-scale response in the high latitudes to major volcanic eruptions (Timmreck 2012; Zanchettin et al. 2012), it is not clear how the ENSO power spectrum from a 50-year time-slice during which a major volcanic eruption occurs would alter compared to the long-term power spectra. Brown et al. (2015) found an increase in variance following the major volcanic eruption of 1258 in four of the six models shown in this study. There are, however, no consistent peaks in the spectral bands around the times of the three major volcanic eruptions in the moving spectra of the palaeo-ENSO reconstructions in Fig. 11.

All of the palaeo-ENSO reconstructions (except Li et al. 2011), a variance reconstruction, show a peak in total spectral power in the late nineteenth century and early twentieth century. Given the wide range of palaeoclimate data used to develop these reconstructions, albeit with some overlap, this provides confidence that there was a change in the ENSO signature at that time. Kestin et al. (1998) reported an increase in variability and spectral power during this period in the observed SOI (see Fig. 7). Stahle et al. (1998) found that there was a statistically significant increase in the interannual variability of SOI in their reconstruction at this time, along with a stronger sea level pressure gradient across the equatorial Pacific. Braganza et al. (2009) also show that there was high variability early in the twentieth century in both the observed SOI and their reconstructed ENSO series with a number of multi-year El Niño and La Niña events. It is unclear if any external forcing drove these changes. The summary of forcing shown in Neukom et al. (2014) suggests the increasing greenhouse gases, increasing solar input after the Maunder and Dalton minima (Lean et al. 2005; Krivova et al. 2010) and the influence of a number of volcanic eruptions including Krakatoa, Indonesia, in 1883 were important.

Previous studies suggested there was reduced ENSO variability from the early fifteenth to middle seventeenth centuries (e.g. Hereid et al. 2012), although it has also been found that it was actually the strength of the teleconnection between ENSO and the ENSO proxy that weakened during that period (Fowler et al. 2012). In this study, rather than a total reduction in the ENSO variance during this period, we observe increased power in the decadal spectral band in the Braganza et al. (2009) and Li et al. (2013) reconstructions around 1600. There is a further peak following this period in the early 1700s in the Braganza et al. (2009), McGregor et al. (2010) and Li et al. (2013) reconstructions. These peaks do not correspond to a consistent signal with the same timing across the climate models, suggesting that they arose from internal variability, or shifts in the teleconnections between ENSO and the climate proxy indicators on which these reconstructions are based.

There is a range of mechanisms that could have driven the changes in spectra seen in this study. Using climate models, the thermocline feedback mechanism and varying zonal wind strength have been found to be major factors influencing ENSO variability (Borlace et al. 2013). Mechanisms to explain the origin of decadal-interdecadal variability in the tropical Pacific include ocean–atmosphere interactions in the North Pacific (e.g. Latif and Barnett 1996), or the combined extratropical-tropical Pacific (e.g. Gu and Philander 1997; Mc Phaden and Zhang 2002; Farneti et al. 2014), and variability within the tropical Pacific domain, including the asymmetry of spatial patterns during El Niño and La Niña (e.g. Yu and Kim 2011 and references therein). All of these mechanisms can contribute to decadal variability in ENSO and its teleconnections (e.g. Power et al. 1999b; An and Wang 2000; Rodgers et al. 2004; Newman et al. 2016). It is quite plausible that changes in these aspects of the climate system arise simply from stochastic

internal variability (e.g. Collins et al. 2010), however, as the ability of climate models to simulate ENSO improves, and they continue to be compared with palaeo-ENSO reconstructions, the response of ENSO to external forcing will become clearer.

6 Summary and conclusions

The recent increases in total spectral power in the last several decades of the observed Nino3.4 and SOI are the highest in the instrumental period. Examining the time-varying spectra of a range of modelled and reconstructed ENSO indices through time, there are epochs when the spectral power has also been significantly high. Thus, the recent increases in power are within the range of modelled or reconstructed variability. However, the observed ongoing increase in atmospheric greenhouse gas levels (Dlugokencky and Tans 2016) provide forcing extending 10 years beyond the end of the Historical simulations, and it is plausible that forcing has led to some of the recent observed increased variance. The observed increased variability maps onto spectral power in the 2–3 years band in both the SOI and Nino3.4 series, but there is only increased power in the decadal band in the SOI, highlighting that ENSO variability can differ depending on the measure used.

Other significant peaks that have occurred throughout the last few centuries include a relative peak in power in the 8–25 years PSD in the early 1700s in the Braganza et al. (2009), McGregor et al. (2010) and Li et al. (2013) palaeo-ENSO reconstructions. The Braganza et al. (2009) and Li et al. (2013) reconstructions also show a peak in the decadal band around 1600. These peaks are not consistent across the results from climate models suggesting that this decadal signature arose from internal variability of the climate system, or shifts in the teleconnections driving the climate indicator on which the reconstructions were based.

The PSD in all bands also increases strongly in the mid-nineteenth century to the early twentieth century in the Braganza et al. (2009), Emile-Geay et al. (2013a, b), Li et al. (2013), McGregor et al. (2010) and Stahle et al. (1998) ENSO reconstructions and the observed Nino3.4 and SOI. The power spectrum from the CCSM4 model also has high relative PSD at the turn of the twentieth century.

The power in the decadal band of the spectra of Nino3.4 from four climate models significantly increased around the time of the major volcanic eruptions of 1258 and 1452, suggesting a forced response in those models. The response in spectra from the palaeo-ENSO reconstructions around the time of the volcanic eruptions was within the range of reconstructed variability. Thus it is unclear if a future major tropical volcanic eruption would drive an increase in power in the decadal band and an epoch when ENSO is more persistently in one phase.

As the ability of climate models to simulate ENSO improves, an increased suite of simulations of the Last Millennium will greatly help in interpreting the results seen across the proxy reconstructions, and extend our understanding of the time-varying characteristics of ENSO variability.

Acknowledgements The contribution of JRB and PH was supported by the Australian Climate Change Science Program. BH acknowledges funding from the Collaborative Research Network (CRN) for 'Self-sustaining Regions Research and Innovation Initiative' and ARC Linkage Project LP150100062. JG is supported by an Australian Research Council Fellowship DE130100668. We acknowledge the World Climate Research Programme's Working Group on Coupled Modelling, which is responsible for CMIP, and we thank the climate modelling groups for producing and making available their model output. For CMIP the U.S. Department of Energy's Program for Climate Model Diagnosis and Intercomparison provides coordinating support and led development of software infrastructure in partnership with the Global Organization for Earth System Science Portals. We also thank the PAGES 2K–PMIP working group for making the ENSO reconstruction dataset readily available. We thank Sophie Lewis for discussion on model evaluation, Francois Delage for help with accessing the climate model data, Karl Braganza for his enthusiasm for exploring spectra, David Karoly for his measured suggestions, and Guomin Wang and Christine Chung for early reviews.

References

Adams JB, Mann M, Ammann C (2003) Proxy evidence for an El Nino-like response to volcanic forcing. Nature 426:274–278

Allan R (2000) ENSO and climatic variability in the past 150 years. In: Diaz H, Markgraf V (eds) El Nino and the Southern Oscillation: multiscale variability and global and regional impacts. Cambridge University Press, Cambridge, pp 3–35

Allan R, D'Arrigo R (1999) 'Persistent' ENSO sequences: how unusual was the 1990–1995 El Nino? The Holocene 9(1):101–118

Allan R, Ansell T (2006) A new globally complete monthly historical gridded mean sea level pressure dataset (HadSLP2): 1850–2004. J Clim 19:5816–5842

Allan R, Nicholls N, Jones P, Butterworth I (1991) A further extension of the Tahiti-Darwin SOI, early SOI results and Darwin pressure. J Clim 4(7):743–749

Allan R, Lindsay J, Parker D (1996) El Nino Southern Oscillation and climate variability. CSIRO, Melbourne

Ammann CM, Joos F, Schimel DS, Otto-Bliesner BL, Tomas RA (2007) Solar influence on climate during the past millennium: results from transient simulations with the NCAR Climate System Model. Proc Natl Acad Sci 104(10):3713–3718

An S, Wang B (2000) Interdecadal change of the structure of the ENSO mode and its impact on the ENSO frequency. J Clim 13:2044–2055

Ault TR, Cole JE, Overpeck JT, Pederson GT, St. George S, Otto-Bliesner B, Woodhouse CA, Deser C (2013) The Continuum of hydroclimate variability in western North America during the Last Millennium. J Clim 26(16):5863–5878

Bellenger H, Guilyardi E, Leloup J, Lengaigne M, Vialard J (2014) ENSO representation in climate models: from CMIP3 to CMIP5. Clim Dyn 42(7–8):1999–2018

Berger A (1978) Long-term variations of daily insolation and Quaternary climatic changes. J Atmos Sci 35:2362–2367
Bjerknes J (1966) A possible response of the atmospheric Hadley circulation to equatorial anomalies of ocean temperature. Tellus 18(4):820–829
Bjerknes J (1969) Atmospheric teleconnections from the equatorial Pacific. Mon Weather Rev 97:163–172
Borlace S, Cai W, Santoso A (2013) Multidecadal ENSO amplitude variability in a 1000-yr simulation of a coupled global climate model: implications for observed ENSO variability. J Clim 26(23):9399–9407
Bradley R (1996) Are there optimum sites for global paleotemperature reconstruction? In: Jones P, Bradley R, Jouzel J (eds) Climate variations and forcing mechanisms of the last 2000 years. Springer, Berlin, pp 603–624
Braganza K, Gergis J, Power S, Risbey J, Fowler A (2009) A multiproxy index of the El Nino–Southern Oscillation, A.D. 1525–1982. J Geophys Res 114(D5):D05106
Briffa K, Jones P (1990) Basic chronology statistics and assessment. In: Cook E, Kairiukstis L (eds) Methods of dendrochronology: applications in the environmental sciences. Kluwer Academic, Dordrecht
Brown JR, Hope P, Gergis J, Henley BJ (2015) ENSO teleconnections with Australian rainfall in coupled model simulations of the Last Millennium. Clim Dyn. doi:10.1007/s00382-015-2824-6
Christensen JH, Krishna-Kumar K, Aldrian E, An SI, Cavalcanti IFA, de Castro M, Dong W, Goswami P, Hall A, Kanyanga JK, Kitoh A, Kossin J, Lau NC, Renwick J, Stephenson DB, Xie SP, Zhou T (2013) Chapter 14: climate phenomena and their relevance for future regional climate change. Climate change 2013: the physical science basis. Contribution of working group I to the fifth assessment report of the intergovernmental panel on climate change. In: Stocker TF, Qin D, Plattner G-K, Tignor M, Allen SK, Boschung J, Nauels A, Xia Y, Bex V, Midgley PM (eds) Cambridge University Press, Cambridge
Cole J, Overpeck J, Cook E (2002) Multiyear La Niña events and persistent drought in the contiguous United States. Geophys Res Lett 29(13):25/1–25/4
Collins M, An S, Cai W, Ganachaud A, Guilyardi E, Jin FF, Jochum M, Lengaigne M, Power S, Timmermann A, Vecchi G, Wittenberg A (2010) The impact of global warming on the tropical Pacific Ocean and El Nino. Nat Geosci 3(6):391–397
Crowley TJ, Unterman MB (2013) Technical details concerning development of a 1200 yr proxy index for global volcanism. Earth Syst Sci Data 5(1):187–197
Deser C, Phillips AS, Tomas RA, Okumura YM, Alexander MA, Capotondi A, Scott JD, Kwon Y-O, Ohba M (2011) ENSO and Pacific decadal variability in the community climate system model version 4. J Clim 25(8):2622–2651
Diaz H, Hoerling M, Eischieid J (2001) ENSO variability, teleconnections and climate change. Int J Climatol 21:1845–1862
Dlugokencky E, Tans P (2016) NOAA/ESRL. http://www.esrl.noaa.gov/gmd/ccgg/trends/
Emile-Geay J, Seager R, Cane M, Cook E, Haug G (2008) Volcanoes and ENSO over the past millennium. J Clim 21(13):3134–3148
Emile-Geay J, Cobb KM, Mann ME, Wittenberg AT (2013a) Estimating central equatorial Pacific SST variability over the past millennium. Part 1: methodology and validation. J Clim 26:2302–2328
Emile-Geay J, Cobb KM, Mann ME, Wittenberg AT (2013b) Estimating central equatorial Pacific SST variability over the past millennium. Part 2: reconstructions and implications. J Clim 26:2329–2352
Farneti R, Molteni F, Kucharski F (2014) Pacific interdecadal variability driven by tropical-extratropical interactions. Clim Dyn 42(11–12):3337–3355
Fernández-Donado L, González-Rouco JF, Raible CC, Ammann CM, Barriopedro D, García-Bustamante E, Jungclaus JH, Lorenz SJ, Luterbacher J, Phipps SJ, Servonnat J, Swingedouw D, Tett S, Wagner S, Yiou P, Zorita E (2013) Large-scale temperature response to external forcing in simulations and reconstructions of the Last Millennium. Clim Past 9:393–421
Flato G et al (2013) Evaluation of climate models. Climate change (2013) The physical science basis. Contribution of working group I to the fifth assessment report of the intergovernmental panel on climate change, In: Stocker TF et al (eds) Cambridge University Press, Cambridge, pp 741–866. www.climatechange2013.org
Fowler AM, Boswijk G, Lorrey A, Gergis J, Pirie M, McCloskey S, Palmer J, Wunder J (2012) Multi-centennial tree-ring record of ENSO-related activity in New Zealand. Nat Clim Change 2(3):172–176
Gao C, Robock A, Ammann C (2008) Volcanic forcing of climate over the past 1500 years: an improved ice core-based index for climate models. J Geophys Res 113(D23):D23111
Gergis J, Fowler A (2005) Classification of synchronous oceanic and atmospheric El Niño–Southern Oscillation (ENSO) events for palaeoclimate reconstruction. Int J Climatol 25:1541–1565
Gergis J, Fowler A (2009) A history of El Niño–Southern Oscillation (ENSO) events since A.D. 1525: implications for future climate change. Clim Change 92(3):343–387
Gergis J, Braganza K, Fowler A, Risbey J, Mooney S (2006) Reconstructing El Nino–Southern Oscillation (ENSO) from high-resolution palaeoarchives. J Quat Sci 21(7):707–722
Glantz MH (2001) Currents of change: impacts of El Niño and La Niña on climate and society. Cambridge Univeristy Press, Cambride
Gu D, Philander G (1997) Interdecadal climate fluctuations that depend on exchanges between the tropics and extratropics. Science 275:805–807
Hanley D, Bourassa M, O'Brian J, Smith S, Spade E (2003) A quantitative evaluation of ENSO indices. J Clim 16:1249–1258
Hereid KA, Quinn TM, Taylor FW, Shen C-C, Lawrence Edwards R, Cheng H (2012) Coral record of reduced El Niño activity in the early 15th to middle 17th centuries. Geology 41(1):51–54
Hourdin F, Foujols M-A, Codron F, Guemas V, Dufresne J-L, Bony S, Denvil S, Guez L, Lott F, Ghattas J, Braconnot P, Marti O, Meurdesoif Y, Bopp L (2013) Impact of the LMDZ atmospheric grid configuration on the climate and sensitivity of the IPSL-CM5A coupled model. Clim Dyn 40(9–10):2167–2192
Jungclaus JH, Giorgetta M, Reick C, Legutke S, Brovkin V, Crueger T, Esch M, Fieg K, Fischer N, Glushak K, Gayler V, Haak H, Hollweg HD, Kinne S, Kornblueh L, Matei D, Mauritsen T, Mikolajewicz U, Müller W, Notz D, Pohlmann T, Raddatz T, Rast S, Roeckner E, Salzmann M, Schmidt H, Schnur R, Segschneider J, Six K, Stockhause M, Wegner J, Widmann H, Wieners K-H, Claussen M, Marotzke J, Stevens B (2012) CMIP5 simulations of the max planck institute for meteorology (MPI-M) based on the MPI-ESM-P model: the past 1000 experiment, served by ESGF. World Data Center Clim. doi:10.1594/WDCC/CMIP5.MXEPpk
Kestin T, Karoly D, Yano JI (1998) Time-frequency variability of ENSO and stochastic simulations. J Clim 11:2258–2272
Kiem AS, Franks SW, Kuczera G (2003) Multi-decadal variability of flood risk. Geophys Res Lett 30(2):1035
Kociuba G, Power SB (2015) Inability of CMIP5 models to simulate recent strengthening of the walker circulation: implications for projections. J Clim 28(1):20–35
Krivova NA, Vieira LEA, Solanki SK (2010) Reconstruction of solar spectral irradiance since the Maunder minimum. J Geophys Res Space Phys 115(A12):A12112

Landrum L, Otto-Bliesner BL, Wahl ER, Conley A, Lawrence PJ, Rosenbloom N, Teng H (2013) Last Millennium climate and its variability in CCSM4. J Clim 26(4):1085–1111

Latif M, Barnett TP (1996) Decadal climate variability over the North Pacific and North America: dynamics and predictability. J Clim 9(10):2407–2423

Lean J, Rottman G, Harder J, Kopp G (2005) SORCE contributions to new understanding of global change and solar variability. In: Rottman G, Woods T, George V (eds) The solar radiation and climate experiment (SORCE). Springer, New York, pp 27–53

Lewis SC, LeGrande AN (2015) Stability of ENSO and its tropical Pacific teleconnections over the Last Millennium. Clim Past 11(10):1347–1360

Li J, Xie SP, Cook ER, Huang G, D'Arrigo R, Liu F, Ma J, Zheng XT (2011) Interdecadal modulation of El Nino amplitude during the past millennium. Nat Clim Change 1:114–118

Li J, Xie S-P, Cook ER, Morales MS, Christie DA, Johnson NC, Chen F, D'Arrigo R, Fowler AM, Gou X, Fang K (2013) El Nino modulations over the past seven centuries. Nat Clim Change 3:822–826

Mann M, Lees J (1996) Robust estimation of background noise and signal detection in climatic time series. Clim Change 33:409–445

Mann M, Zhang Z, Rutherford S, Bradley R, Hughes M, Shindell D, Ammann C, Faluvegi G, Ni F (2009) Global signatures and dynamical origins of the little ice age and medieval climate anomaly. Science 326:1256–1260

Mc Phaden M, Zhang D (2002) Slowdown of the meridional overturning circulation in the upper Pacific ocean. Nature 415:603–608

McGregor S, Timmermann A (2011) The effect of explosive tropical volcanism on ENSO. J Clim 24(8):2178–2191

McGregor S, Timmermann A, Timm O (2010) A unified proxy for ENSO and PDO variability since 1650. Clim Past 6:1–17

McGregor S, Timmermann A, England MH, Elison Timm O, Wittenberg AT (2013) Inferred changes in El Niño–Southern Oscillation variance over the past six centuries. Clim Past 9(5):2269–2284

Neukom R, Gergis J, Karoly D, Wanner H, Curran M, Elbert J, González-Rouco F, Linsley B, Moy A, Mundo I, Raible C, Steig E, van Ommen T, Vance T, Villalba R, Zinke J, Frank D (2014) Inter-hemispheric temperature variability over the Last Millennium. Nat Clim Change 4:362–367

Newman M, Alexander MA, Ault TR, Cobb KM, Deser C, Di Lorenzo E, Mantua NJ, Miller AJ, Minobe S, Nakamura H, Schneider N (2016) The Pacific decadal oscillation, revisited. J Clim. doi:10.1175/JCLI-D-15-0508.1

Nicholls N (1988) Low latitude volcanic eruptions and the El Nino–Southern Oscillation. J Climatol 8:91–95

Ohba M, Shiogama H, Yokohata T, Watanabe M (2013) Impact of strong tropical volcanic eruptions on ENSO simulated in a coupled GCM. J Clim 26(14):5169–5182

Percival DB, Walden AT (1993) Spectral analysis for physical applications: multitaper and conventional univariate techniques. Cambridge University Press, Cambridge

Phipps SJ, Rotstayn LD, Gordon HB, Roberts JL, Hirst AC, Budd WF (2012) The CSIRO Mk3L climate system model version 1.0-part 2 response to external forcings. Geosci Model Dev 5(3):649–682

Phipps S, McGregor H, Gergis J, Gallant AJE, Neukom R, Stevenson S, van Ommen T, Brown J, Fischer M, Ackerley D (2013) Paleoclimate data-model comparison: concepts, uncertainties and application to the climate of the past 1500 years. J Clim 26:6915–6936

Pongratz J, Reick C, Raddatz T, Claussen M (2008) A reconstruction of global agricultural areas and land cover for the Last Millennium. Glob Biogeochem Cycles 22:3018. doi:10.1029/2007gb003153

Power S, Colman R (2006) Multi-year predictability in a coupled general circulation model. Clim Dyn 26(2–3):247–272

Power S, Kociuba G (2011) The impact of global warming on the Southern Oscillation Index. Clim Dyn 37(9–10):1745–1754

Power S, Casey T, Folland C, Colman A, Mehta V (1999a) Inter-decadal modulation of the impact of ENSO on Australia. Clim Dyn 15:319–324

Power S, Tseitkin F, Mehta V, Lavery B, Torok S, Holbrook N (1999b) Decadal climate variability in Australia during the twentieth century. Int J Climatol 19:169–184

Rasmusson E, Carpenter T (1982) Variations in tropical sea surface temperature and surface wind fields associated with the Southern Oscillation/El Nino. Mon Weather Rev 110:354–384

Rasmusson E, Wallace J (1983) Meteorological aspects of the El Nino/Southern Oscillation. Science 222:1195–1202

Rayner NA, Parker DE, Horton EB, Folland CK, Alexander LV, Rowell DP, Kent EC, Kaplan A (2003) Global analyses of sea surface temperature, sea ice, and night marine air temperature since the late nineteenth century. J Geophys Res. doi:10.1029/2002JD002670

Rodgers KB, Friederichs P, Latif M (2004) Tropical Pacific decadal variability and its relation to decadal modulations of ENSO. J Clim 17(19):3761–3774

Ropelewski CF, Jones PD (1987) An extension of the Tahiti-Darwin Southern Oscillation Index. Mon Weather Rev 115:2161–2165

Sato M, Hansen JE, McCormick MP, Pollack JB (1993) Stratospheric aerosol optical depths, 1850–1990. J Geophys Res Atmos 98(D12):22987–22994

Schmidt GA, Ruedy R, Hansen JE, Aleinov I, Bell N, Bauer M, Bauer S, Cairns B, Canuto V, Cheng Y, Del Genio A, Faluvegi G, Friend AD, Hall TM, Hu Y, Kelley M, Kiang NY, Koch D, Lacis AA, Lerner J, Lo KK, Miller RL, Nazarenko L, Oinas V, Perlwitz J, Perlwitz J, Rind D, Romanou A, Russell GL, Sato M, Shindell DT, Stone PH, Sun S, Tausnev N, Thresher D, Yao M-S (2006) Present-day atmospheric simulations using giss model E: comparison to in situ, satellite, and reanalysis data. J Clim 19(2):153–192

Schmidt GA, Jungclaus JH, Ammann CM, Bard E, Braconnot P, Crowley TJ, Delaygue G, Joos F, Krivova NA, Muscheler R, Otto-Bliesner BL, Pongratz J, Shindell DT, Solanki SK, Steinhilber F, Vieira LEA (2011) Climate forcing reconstructions for use in PMIP simulations of the Last Millennium (v1.0). Geosci Model Dev 4(1):33–45

Schmidt GA, Jungclaus JH, Ammann CM, Bard E, Braconnot P, Crowley TJ, Delaygue G, Joos F, Krivova NA, Muscheler R, Otto-Bliesner BL, Pongratz J, Shindell DT, Solanki SK, Steinhilber F, Vieira LE (2012) Climate forcing reconstructions for use in PMIP simulations of the Last Millennium (v1.1). Geosci Model Dev 5:185–191

Stahle D, D' Arrigo R, Krusic P, Cleaveland M, Cook E, Allan R, Cole J, Dunbar R, Therrell M, Gay D, Moore M, Stokes M, Burns B, Villanueva-Diaz J, Thompson L (1998) Experimental dendroclimatic reconstruction of the Southern Oscillation. Bull Am Meteorol Soc 79(10):2137–2152

Stevenson S, Otto-Bliesner B, Fasullo J, Brady E (2016) "El Niño-like" hydroclimate response to Last Millennium volcanic eruptions. J Clim 29:2907–2921

Sueyoshi T, Ohgaito R, Yamamoto A, Chikamoto MO, Hajima T, Okajima H, Yoshimori M, Abe M, O'Ishi R, Saito F, Watanabe S, Kawamiya M, Abe-Ouchi A (2013) Set-up of the PMIP3 paleoclimate experiments conducted using an earth system model, MIROC-ESM. Geosci Model Dev 6(3):819–836

Taylor KE, Stouffer RJ, Meehl GA (2012) An overview of CMIP5 and the experiment design. Bull Am Meteorol Soc 93(4):485–498

Thomson DJ (1982) Spectrum estimation and harmonic analysis. Proc IEEE 70(9):1055–1096

Timmreck C (2012) Modeling the climatic effects of large explosive volcanic eruptions. Wiley Interdiscip Rev Clim Change 3(6):545–564

Troup A (1965) The Southern Oscillation. Q J R Meteorol Soc 91:490–506

Vecchi GA, Wittenberg AT (2010) El Niño and our future climate: where do we stand? Wiley Interdiscip Rev Clim Change 1(2):260–270

Vieira L, Solanki S (2009) Evolution of the solar magnetic flux on time scales of years to millennia. Astron Astrophys. doi:10.1051/0004-6361/200913276

Wang YM, Lean JL, Sheeley NR Jr (2005) Modeling the Sun's magnetic field and irradiance since 1713. Astrophys J 625(1):522–538

Watanabe S, Hajima T, Sudo K, Nagashima T, Takemura T, Okajima H, Nozawa T, Kawase H, Abe M, Yokohata T, Ise T, Sato H, Kato E, Takata K, Emori S, Kawamiya M (2011) MIROC-ESM 2010: model description and basic results of CMIP5-20c3m experiments. Geosci Model Dev 4(4):845–872

Welch PD (1967) The use of fast Fourier Transform for the estimation of power spectra: a method based on time averaging over short, modified periodograms. IEEE Trans Audio Electroacoust 15(2):70–73

Wilson R, Cook E, D'Arrigo R, Riedwyl N, Evans M, Tudhope A, Allan R (2010) Reconstructing ENSO: the influence of method, proxy data, climate forcing and teleconnections. J Quat Sci 25(1):62–78

Wittenberg AT (2009) Are historical records sufficient to constrain ENSO simulations? Geophys Res Lett 36(12):L12702

Wittenberg AT, Rosati A, Lau N-C, Ploshay JJ (2006) GFDL's CM2 global coupled climate models. Part III: tropical Pacific climate and ENSO. J Clim 19(5):698–722

Xin XG, Wu TW, Zhang J (2013) Introduction of CMIP5 experiments carried out with the climate system models of Beijing Climate Center. Adv Clim Change Res 4(1):41–49

Yan H, Sun L, Wang Y, Huang W, Qiu S, Yang C (2011) A record of the Southern Oscillation Index for the past 2000 years from precipitation proxies. Nat Geosci 4:611–614

Yu J-Y, Kim ST (2011) Reversed spatial asymmetries between El Niño and La Niña and their linkage to decadal ENSO modulation in CMIP3 models. J Clim 24(20):5423–5434

Zanchettin D, Timmreck C, Graf H-F, Rubino A, Lorenz S, Lohmann K, Krüger K, Jungclaus JH (2012) Bi-decadal variability excited in the coupled ocean–atmosphere system by strong tropical volcanic eruptions. Clim Dyn 39(1):419–444

Zhang D, Blender R, Fraedrich K (2013) Volcanoes and ENSO in millennium simulations: global impacts and regional reconstructions in East Asia. Theor Appl Climatol 111(3):437–454